CEBAF Program Advisory Committee Eight Cover Sheet

This proposal must be received by close of business on Thursday, April 14, 1994 at:

CEBAF
User Liaison Office, Mail Stop 12 B
12000 Jefferson Avenue
Newport News, VA 23606

Proposal Title

Measurement of the Deuteron Tensor Polarization at Large Momentum Transfers in D(e,e'd) Scattering

Contact Person

Name: Serge Kox
Institution: Institut des Sciences Nucléaires, Grenoble
Address: IN2P3-UJF
Address: F-38026 Grenoble Cedex
City, State ZIP/Country: France
Phone: (33)76 28 40 00 **FAX:** (33)76 28 40 04
E-Mail → Internet: KOX@FRCPN11.IN2P3.FR

Experimental Hall: C
Total Days Requested for Approval: 46
Minimum and Maximum Beam Energies (GeV): 1.3 - 4.0
Minimum and Maximum Beam Currents (μAmps): 50 - 100 μA

CEBAF Use Only

Receipt Date: 4/14/94 PR 94-018

By: Lo Anick

Proposal for CEBAF PAC 8 (June 1994)

Measurement of the Deuteron Tensor Polarization at Large Momentum Transfers in $\mathbf{D}(e, e' \vec{d})$ Scattering

T. Aniel [d], J. Arvieux [d], G. Audit [b], E.J. Beise [g], A. Betker [f], L. Bimbot [c], E. Brash [e*], H. Breuer [g], J.M. Cameron [f], R. Carlini [j], N.S. Chant [g], C.C. Chang [g], C. Djalali [c], G.W. Dodson [h], K. Dow [h], F. Duncan [g], J.E. Ducret [b], M. Farkhondeh [h], B. Frois [b], C. Furget [a], M. Garçon [b], R. Gilman [e], C. Glashausser [e], J. Jourdan [i], S. Kox [a], D. Mack [j], P. Markowitz [g], S. Platchkov [b], R. Ransome [e], J.S. Real [a], P.G. Roos [g], P. Rutt [e], A. Saha [j], W. Schmitt [f], E.J. Stephenson [f], E. Tomasi-Gustaffson [d], W. Turchinetz [h], E. Voutier [a], S.A. Wood [j], C. Yan [j]

[a] Institut des Sciences Nucléaires, IN2P3-UJF, F-38026 Grenoble Cedex, France

[b] DAPNIA/Service de Physique Nucléaire, CEN Saclay, F-91191 Gif-sur-Yvette, France

[c] Institut de Physique Nucléaire, F-91400 Orsay, France

[d] Laboratoire National Saturne, IN2P3–CNRS and DSM–CEA, F-91191 Gif-sur-Yvette, France

[e] Rutgers University, Box 849, Piscataway, NJ 08854, USA

[f] IUCF, Bloomington, IA 47405, USA

[g] University of Maryland, College Park, MD 20742, USA

[h] MIT/Bates, Cambridge, MA, 02139, USA

[i] Institut fuer Physik, CH-4056 Basel, Switzerland

[j] CEBAF, Newport News, VA 23606, USA

S. Kox (spokesperson) and E.J. Beise (co-spokeperson)

94-015

ABSTRACT

We propose to extend the existing measurements of the deuteron tensor polarization, t_{20}, produced in the D(e, $e'\vec{d}$) scattering. Using the HMS spectrometer in Hall C and a new deuteron tensor polarimeter (*POLDER*), t_{20} will be measured in the range of four-momentum transfer $Q = 4.0 - 6.8$ fm^{-1}. When combined with knowledge of the elastic structure functions A and B, this quantity permits the separation of the charge (G_C) and quadrupole (G_Q) form factors of the deuteron. The determination of G_C at large momentum transfer will test the applicability of existing theoretical models and their assumptions, and help determine the effects of non-nucleonic degrees of freedom.

April 13, 1994

1 Introduction

The deuteron has spin 1, and its electromagnetic structure is therefore described by three form factors: the charge monopole G_C, charge quadrupole G_Q and magnetic dipole G_M. Non-relativistically, these form factors are related to the spatial distributions of charge, quadrupole deformation and magnetization respectively, both the nucleon spins and the nucleon currents contributing to the latter.

Many models of the deuteron electromagnetic form factors have been proposed. In the impulse approximation (IA) description of *e-d* scattering, the electron interacts with each nucleon in the deuteron via a virtual photon and the electromagnetic form factors of the interacting nucleon are taken to be the same as those for a free nucleon. At large four-momentum transfers, corrections to the IA model become important. These include isoscalar meson-exchange currents (MEC), isobar components (IC), relativistic effects and perhaps quark degrees of freedom.

Experimentally, at least three observables of *e-d* scattering are needed to separate all three form factors (see section 2). Differential cross section measurements at different electron angles for the same four-momentum transfer allow the determination of the longitudinal and transverse structure functions $A(G_C^2, G_Q^2, G_M^2)$ and $B(G_M^2)$, which so far have been the main testing ground for the theoretical models. A is measured up to $Q = 10$ fm^{-1} [1] and B up to $Q = 8$ fm^{-1} [2]. To separate further G_C and G_Q, the measurement of another observable is required, and this is necessarily a polarization observable. One must either measure the asymmetries induced by a tensor polarized deuterium target, or measure the tensor polarization of the recoil deuterons[1]. The tensor moments are a measure of the relative probabilities of scattering off deuterons in magnetic substates $m_z = +1, -1$ or 0 when dealing with a polarized target (T_{2q}), or of producing deuterons in these different magnetic substates when measuring the polarization (t_{2q}) of the outgoing deuterons. When combined with $A(G_C{}^2, G_Q{}^2, G_M{}^2)$ and $B(G_M{}^2)$, $t_{20}(G_C, G_Q, G_M, \theta_e)$ allows the separate determination of the two charge form factors G_C and G_Q (θ_e is the electron scattering angle). The two other tensor moments t_{21} and t_{22} provide other useful quadratic combinations of the form factors. Contrary to all other observables and to the deuteron form factors themselves, t_{20} is nearly independent of the elementary nucleon form factors, and in particular of the poorly known neutron electric form

[1] alternatively, one may deal with deuteron vector polarization only if the electron beam is also polarized; this type of experiment has never been attempted, but is not expected to yield a better determination of the individual form factors [8].

factor.

We propose here to perform new precise measurements of t_{20} , t_{21}, and t_{22} at $4.0 < Q < 6.8$ fm^{-1}. These measurements will both determine with better accuracy the behaviour of G_C around its passage through zero and extend the separate determination of G_C and G_Q to regions where quark degrees of freedom may begin to play a more significant role in the description of the deuteron. Six measurements can be made with 46 days of 100 μA beam in Hall C, using the HMS to detect electrons and a specially designed magnetic channel to detect deuterons in coincidence. The deuteron tensor polarization will be determined with a new polarimeter (*POLDER* [10]) which relies on the $p(d,2p)n$ reaction which has a large figure of merit for $175 < T_d < 500$ MeV. This polarimeter is thus ideally suited for the Q-range of t_{20} which can be addressed at CEBAF beam energies.

This experiment was originally proposed to PAC 6 last year (PR-93-003). Although the PAC responded enthusiastically to the physics of the experiment, the proposal was deferred (the PAC 6 report is attached to this document). The main questions brought up by PAC 6 were whether or not the deuteron channel and kinematics were optimized for the best use of beam time, and whether backgrounds in the polarimeter were investigated in sufficient detail to determine the feasibility of the required precision $p(d,2p)n$ cross section measurement. Since PAC 6, we have addressed both of these issues in considerable detail, and believe that this proposal represents an optimized use of CEBAF beam with adequate control and understanding of possible backgrounds.

The proposal is organized as follows. The next section will introduce the kinematics and relevant observables, followed in section 3 by a description of previous measurements and different physical models of the deuteron in comparison with the existing data. The experiment will then be described in detail, concluding with an updated beam request and a list of collaboration responsibilities.

2 Kinematics and Observables

In elastic e-d scattering, the energies of the incident (E_e) and scattered (E'_e) electrons and the kinetic energy of the scattered deuteron (T_d) are related to Q by:

$$Q^2 = 2\,M_d\,T_d = 2\,M_d\,(E_e - E'_e) = 4E_eE'_e sin^2\left(\frac{\theta_e}{2}\right) \qquad (2.1)$$

where M_d is the deuteron mass and θ_e the scattering angle of the electron.

It is also convenient to express the angular correlation as:

$$\sin^2(\theta_d) = \frac{\cos^2\left(\frac{\theta_e}{2}\right)}{1+\mu\sin^2\left(\frac{\theta_e}{2}\right)} \Longleftrightarrow \sin^2(\theta_e) = \frac{\cos^2\left(\frac{\theta_d}{2}\right)}{1+\mu\sin^2\left(\frac{\theta_d}{2}\right)} \tag{2.2}$$

with

$$\mu = \left(\frac{E_e}{M_d}\right)^2 + \frac{2E_e}{M_d} \tag{2.3}$$

By using the first Born approximation (one-photon exchange approximation) and imposing relativistic and gauge invariance, the differential cross section can be written as:

$$\frac{d\sigma}{d\Omega} = \left(\frac{d\sigma}{d\Omega}\right)_{Mott} \cdot S \tag{2.4}$$

where

$$\left(\frac{d\sigma}{d\Omega}\right)_{Mott} = \frac{E'_e}{E_e} \cdot \frac{\alpha^2\cos^2\frac{\theta_e}{2}}{4E_e^2\sin^4\frac{\theta_e}{2}} \tag{2.5}$$

describes the scattering of an electron off a pointlike spinless particle (α is the fine structure constant), and

$$S = A(Q) + B(Q)\tan^2\frac{\theta_e}{2} \tag{2.6}$$

originates from the electromagnetic structure of the deuteron. As a consequence of parity and time-reversal invariance, the structure functions A and B are in turn given in terms of three elementary electromagnetic form factors:

$$A(Q) = G_C^2(Q) + \frac{8}{9}\eta^2 G_Q^2(Q) + \frac{2}{3}\eta G_M^2(Q) \tag{2.7}$$

$$B(Q) = \frac{4}{3}\eta(1+\eta)G_M^2(Q) \tag{2.8}$$

with $\eta = Q^2/4M_d^2$.

The three moments t_{2q} of the deuteron tensor polarization are given by:

$$t_{20} = -\frac{1}{\sqrt{2}\,S}\left[\frac{8}{3}\eta G_C G_Q + \frac{8}{9}\eta^2 G_Q^2 + \frac{1}{3}\eta[1+2(1+\eta)\tan^2\frac{\theta_e}{2}]G_M^2\right] \tag{2.9}$$

$$t_{21} = \frac{2}{\sqrt{3}\,S}\,\eta[\eta+\eta^2\sin^2\frac{\theta_e}{2}]^{1/2} G_M G_Q \sec\frac{\theta_e}{2} \tag{2.10}$$

$$t_{22} = -\frac{1}{2\sqrt{3}\,S}\,\eta G_M^2 \tag{2.11}$$

In the one photon-exchange approximation of e-d scattering, and as a result of time-reversal invariance, the deuteron vector polarization is identically zero when using an unpolarized electron beam.

The form factors are normalized at $Q = 0$ to the static moments:

$$G_C(0) = 1 \tag{2.12}$$

$$G_Q(0) = M_d^2 \mathcal{Q}_d = 25.83 \tag{2.13}$$

$$G_M(0) = \frac{M_d}{M_p}\mu_d = 1.714 \tag{2.14}$$

where $\mathcal{Q}_d$ and μ_d are respectively the electric quadrupole moment and the magnetic dipole moment of the deuteron, and M_p is the proton mass.

The quantity $\tilde{t}_{20}$, derived from Eq. 2.9 by neglecting the magnetic contribution is often used in the literature. Though not an observable, it is interesting since it depends solely on the ratio

$$x = \frac{2}{3}\eta G_Q/G_C \tag{2.15}$$

$$\tilde{t}_{20} = -\sqrt{2}\,\frac{x(x+2)}{1+2x^2} \tag{2.16}$$

At small four-momentum transfers, $x \ll 1$ and $t_{20} \simeq \tilde{t}_{20} \simeq -2x\sqrt{2} \simeq -\frac{\sqrt{2}}{3}\mathcal{Q}_d Q^2$, so that t_{20} is constrained by the known deuteron quadrupole moment. The maximum difference between t_{20} and $\tilde{t}_{20}$ occurs around their absolute minimum (*i.e.*, when x=1). For our proposed measurement, where electron angles are small, the difference between t_{20} and $\tilde{t}_{20}$ is at most 0.1.

3 Physics Motivation

Measurements of t_{20} [3, 4, 5, 6, 7, 9, 12] have been performed up to a four-momentum transfer of $Q = 4.6$ fm^{-1}, and are shown in figure 1 along with selected theoretical curves. At relatively low momentum transfer ($Q < 3$ fm^{-1}), t_{20} is well determined by the non-relativistic impulse approximation with small theoretical uncertainties. The two most recent experiments to be completed have extended the measurements into a range where theoretical models differ significantly in their predictions for t_{20}. One was an experiment at Bates, with the polarimeter AHEAD [11]. All three moments of the recoil deuteron tensor polarization (t_{20}, t_{21} and t_{22}) were extracted at $3.8 < Q < 4.6$ fm^{-1} [9]. The second experiment, performed with a polarized target in the Novosibirsk storage ring, measured the tensor analyzing power

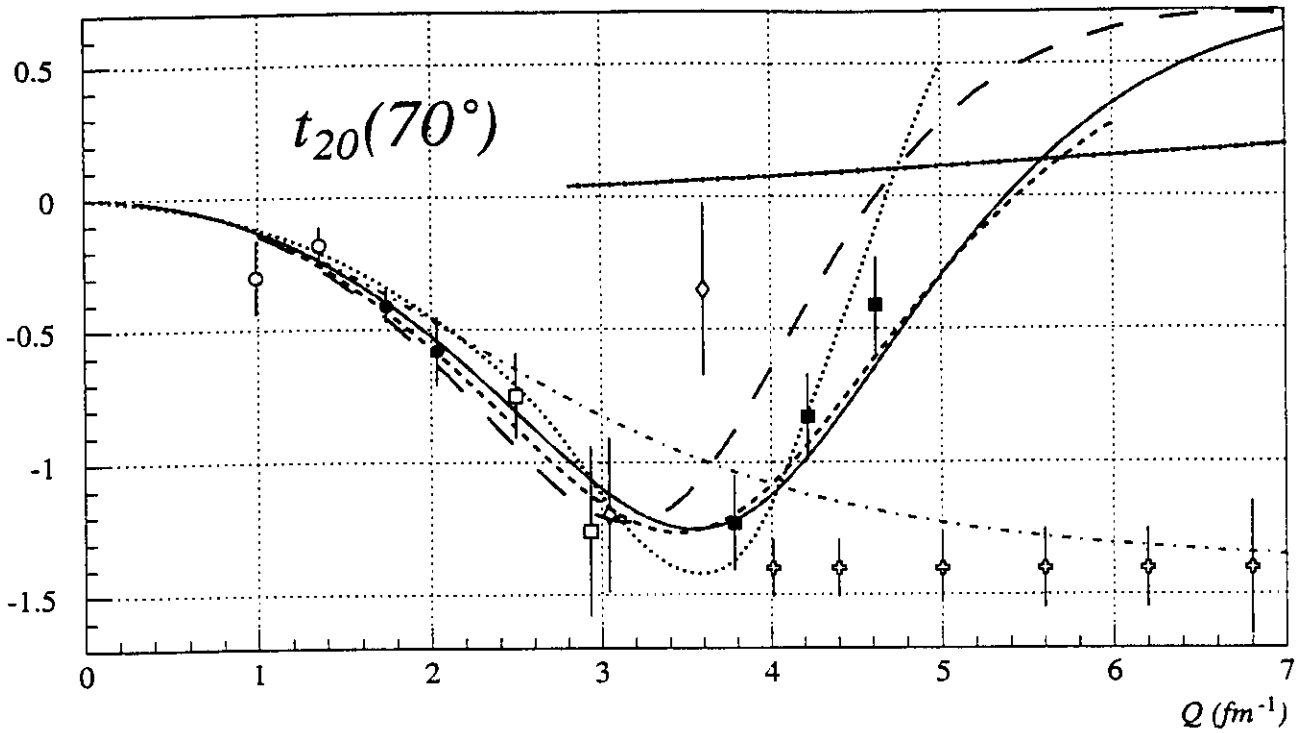

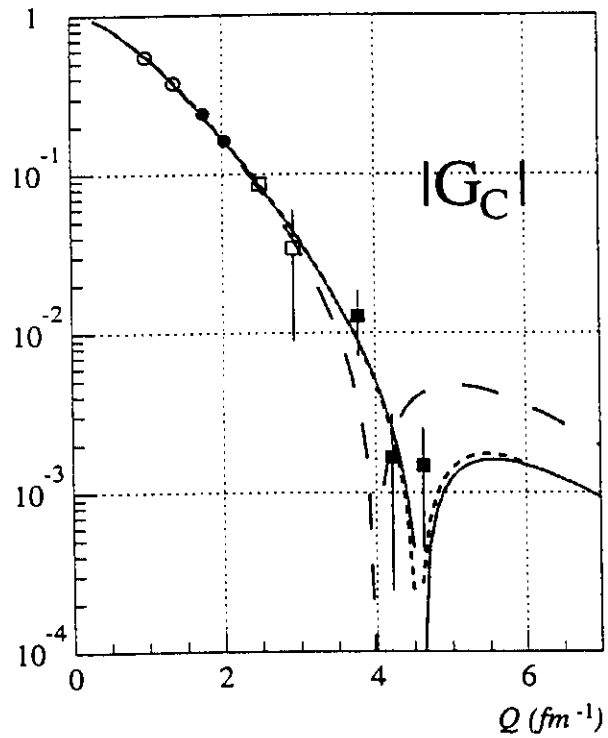

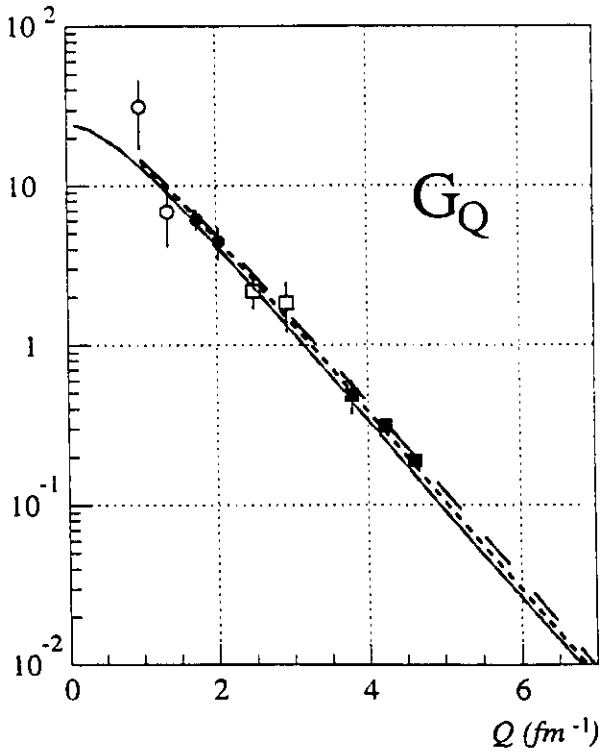

- Bates (1984)
- Novosibirsk (1985)
- Novosibirsk (1990)
- Bates (1991)
- Novosibirsk (1993)
- expected at CEBAF

------ NRIA (Schiavilla-Riska)
— – NRIA + MEC + RC (Schiavilla-Riska)
——— RIA + MEC (Hummel-Tjon)
..... Skyrme (Nyman-Riska)
- - - - - PQCD (Carlson)
——— PQCD (Brodsky-Hiller)

figure 1

T_{20}. Preliminary data [12] are available from this experiment, and where the two measurements overlap they differ significantly in the extracted value of t_{20}. These two experiments were performed using very different techniques with very different systematic errors, and thus demonstrate the need for complementary measurements, and for additional precise measurements in this region of momentum transfer. More measurements at Novosibirsk are currently underway but will only provide data for Q smaller than 5 fm^{-1} . The experiment proposed here will also add data in this region.

3.1 Models

In the NRIA, the deuteron charge form factor $G_C(Q)$ has a structure very similar to $u(k)$, the s-state wave function in momentum space, with k, the momentum of the nucleons with respect to their center of mass, equal to $Q/2$ [13]. The Bates experiment provided the first experimental evidence for a node in G_C(located around 4.4 fm^{-1}). This node is a reflection of a node in the s-state wave function, which is in turn due to the repulsive nature of the NN interaction at short distances. The weaker the short-range repulsion of the NN potential, the more the node of $u(k)$ will move to higher values, the shallower the minimum of G_C and the less steep the slope of t_{20} will appear. At the limit where the hard core disappears, the node moves to infinity and $\bar{t}_{20}$ remains lower than $-1/\sqrt{2}$. NN potentials developed in the last ten years all incorporate the main features of the NN scattering data. But phase-shift equivalence does not imply equal potential or wave-function, and therefore differences may manifest themselves in the deuteron form factors. Calculations of the deuteron form factors and e-d observables in the NRIA have been performed by many authors [14]–[19]. With realistic NN potentials, the NRIA gives a fair description of the existing data.

However, near the node of G_C at 4–5 fm^{-1}, the measured structure function A determines mostly G_Q. Short-range components, non-nucleonic contributions and relativistic effects become important at this momentum transfer, and manifest themselves mainly in G_C. Thus t_{20} is significantly more sensitive to these effects than is A in this region. Different theoretical descriptions of t_{20} incorporate these effects in various ways. A complete description of available models is given in both the previous version of this proposal (PAC 6) and in ref. [9], and will not be described in detail here. However, a brief description is provided in order to highlight some of the outstanding features in comparison with the data.

Isoscalar meson exchange calculations include pair and retardation currents, where the pion contribution largely dominates over that of heavier mesons, as well as model-dependent $\rho\pi\gamma$ and $\omega\sigma\gamma$ contributions. Most MEC calculations also include various relativistic one- and two-body current contributions (RC) added perturbatively to the NRIA results. As compared with NRIA, the minimum of G_C is shifted to lower Q values. This shift is larger than the Bates data would suggest (except in the case where the Bonn-E potential is used [20]), but smaller than suggested by the Novosibirsk data. In the three-body system, such MEC contributions are required [21, 22] in order to reproduce the isoscalar charge form factor extracted from e-^{3}He and e-^{3}H elastic scattering [23].

Relativistic models have been developed in both the Light Cone formalism and solving a Bethe-Salpeter equation. Most do not include contributions from MEC such as the $\rho\pi\gamma$ process and are therefore referred to as relativistic impulse approximation (RIA). However the pair and retardation currents are included automatically in some models of RIA [24, 25]. Hummel and Tjon [26] performed a relativistically covariant analysis of $\rho\pi\gamma$ and $\omega\sigma\gamma$ MEC's, which were treated consistently with the NN dynamics within a quasipotential one-boson-exchange (OBE) model. They derived the relativistic formulae for the $\rho\pi\gamma$ and $\omega\sigma\gamma$ current operators and evaluated their matrix elements using a relativistic OBE model with $\pi, \rho, \omega, \sigma, \eta$ and δ mesons. They find the $\rho\pi\gamma$ contribution to the form factors to be much smaller than in the non-relativistic case, and consequently the $\omega\sigma\gamma$, thus far never considered, of comparable importance. The RIA is in agreement with the Bates data, while the addition of the MEC changes the results by less than one experimental error bar. The $\rho\pi\gamma$ and $\omega\sigma\gamma$ contributions to G_Q almost exactly cancel each other, while the $\omega\sigma\gamma$ contribution to G_C is twice as large, with opposite sign, as the $\rho\pi\gamma$ one. The same authors [27] investigated a different approximation for the nucleon propagators occuring at the electromagnetic vertex: measurable differences of the order of 0.3 in t_{20} are found around $Q = 6$ fm^{-1}. Similar relativistically covariant calculations have been performed by Devine [28], with equally good agreement with the Bates data.

Relativistic calculations using the Light Cone formalism have also been performed, and give a good description of the data. The problem of including MEC has not yet been dealt with in this approach.

At high momentum transfer ($Q > 5$ fm^{-1}), the deuteron is probed at smaller internucleon distances and the quark substructure should manifest itself in the deuteron observables. Quark configurations are incorporated in several hybrid quark-

hadron models with a quark confinement radius taken as a free parameter. Some of them give predictions similar to those of the IA model while others have completely different results for the high four-momentum transfer region. Within these models, the form factors seem to be very sensitive both to the $6q$ configurations being used and to the dynamical connection between the $6q$ and NN configurations.

In Skyrme models, baryons are soliton solutions (Skyrmions) of a Lagrangian constructed on a SU(2) field. The isoscalar electromagnetic current operator is proportional to the anomalous baryon current operator which depends on the fields of the Lagrangian but not on their interaction. The current operator for the deuteron can be expressed as a sum of the isoscalar current operator of single nucleons and an irreducible two-body exchange operator. This exchange current has been formally identified [29] with the conventional $\rho\pi\gamma$ MEC. Nyman and Riska [30] predicted the deuteron electromagnetic form factors with a Skyrme model, using a deuteron wave function generated from the Paris NN potential. Their results give a steeper slope to t_{20} than most other models (see figure 1). Such a behavior will be tested in the experiment proposed here.

At sufficiently large momentum transfer, PQCD is expected to become applicable. Brodsky and collaborators studied the high-Q behaviour of the electromagnetic form factors of nucleons and of the deuteron within the framework of PQCD. They derived the quark counting rule which predicts, for the deuteron, $\sqrt{A(Q)} \propto Q^{-10}$ as $Q \to \infty$. Carlson and Gross [31] showed that, though classical nuclear physics may lead to the same power law, spin observables could provide the distinctive signature that $\tilde{t}_{20}$ approaches the constant value of $-\sqrt{2}$ at large Q. Carlson [32] later suggested that this asymptotic behaviour could be matched to the low momentum transfer limit by the *adhoc* construction: $G_C = (1/M_d^2 Q_d + \frac{2}{3}\eta)G_Q$. Brodksy and Hiller [33] reexamined the asymptotic behaviour of the deuteron form factors, claiming that the relevant momentum transfer scale is $Q \gg \sqrt{2M_d\Lambda_{QCD}} \sim 4.5$ fm^{-1} (with $\Lambda_{QCD} \sim 200$ MeV), much lower than the scale usually given by $\eta \gg 1$. A test of the applicability of PQCD to the description of the charge form factors will then be to determine whether t_{20} flattens out to near zero above 5 fm^{-1}. Most other models predict that t_{20} will reach its absolute maximum around 6 or 7 fm^{-1} , while the Brodksy and Hiller prediction is that this occurs at $Q = 13.4$ fm^{-1}. This approach was recently improved by Kobushkin and Syamtomov [34] who predict t_{20} of the order of -0.25 in the range of our proposed measurements.

4 The Experiment

The goal of this experiment is to extend the measurements of t_{20} to higher values of Q ($4.0 < Q < 6.2$ fm^{-1}) with good precision. Additional data with more modest precision will be obtained at $Q = 6.8$ fm^{-1}. The preceding section illustrates that such data are needed to test the validity of various theoretical models and to help discriminate between different physical descriptions of the two-nucleon system. It is also important to add points with improved precision to better determine the node of G_C and to check the present discrepancy between the Bates and the Novosibirsk data [12].

A schematic of the general experimental setup is shown in figure 2. The experiment will require two spectrometers triggered in coincidence for the simultaneous detection of the scattered electron and recoiling deuteron. The polarization of the recoil deuterons will be measured in the polarimeter *POLDER*, in which the two outgoing protons from the $p(d, 2p)n$ reaction are detected. The range of operation of this new polarimeter (deuteron kinetic energies of 175−500 MeV) allows one to perform measurements in the range of four-momentum transfer Q from $4.0 - 6.8$ fm^{-1} (see Eq. 2.1).

Because this is a double scattering experiment and the e-d cross sections are small (of the order of 0.01 nb/sr), a thick liquid deuterium target, large acceptances for the electron and deuteron spectrometers, and a high efficiency for the deuteron polarimeter are required to obtain good statistical accuracy in a reasonable amount of beam time. We propose to use a 12 cm long liquid deuterium target with 100 μA of beam; therefore a high power cryogenic system (400 W) will be needed for the target. The details of the target system will be discussed in detail in section 4.4.

This experiment could be performed either in Hall A or C, using either the HRS or the HMS spectrometer for the detection of the electron. For the deuteron magnetic channel, none of the existing spectrometers at CEBAF is really appropriate. A very dispersive magnetic channel would lead to a large kinematical mismatch factor between the electron arm and the deuteron arm, and consequently to a prohibitive beam time request. Thus we propose to develop a specific device (see section 4.3) placed at a fixed angle.

Although the requirements on the electron arm are not particularly specialized, the availability of power supplies, shielding, and cooling water for the deuteron channel make Hall C the most favorable location at this time. We have therefore written the proposal assuming the experiment would be run in Hall C.

Deuteron Channel

(CEBAF - Hall C - t_{20} experiment)

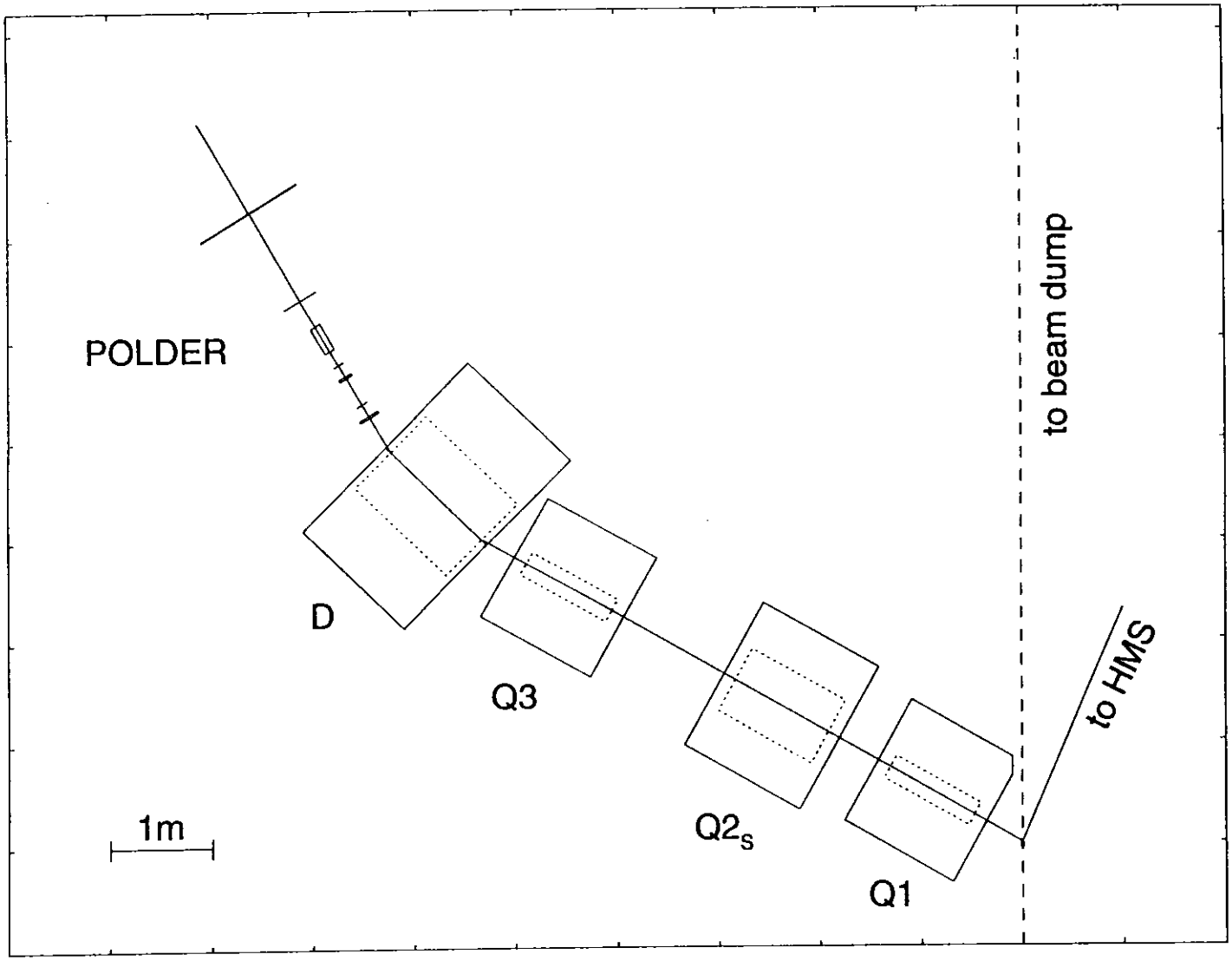

figure 2

4.1 Beam Energy and Intensity

A high beam intensity is required in this experiment. At the lowest energy kinematics, limitations in luminosity arise from the rate of background charged particles reaching the polarimeter. At the highest energy, background rates in the polarimeter will be rather modest, but power dissipated by the beam in the LD_2 target is a constraint. It appears that a beam intensity of 100 μA can be achieved with a modest upgrade to the Hall C target, and thus this value was used in making beam time estimates.

Since the experiment will be performed at a fixed deuteron angle, the beam energy will be changed for the different values of momentum transfer. The choice of beam energy has been driven by several factors. For a perfect kinematical match between the deuteron and electron arms, the counting rate would increase with E^2. However, as the beam energy increases, several disadvantages arise. Background rates in both the electron and deuteron arms increase. In addition, the range of momentum transfer taken in one electron spectrometer setting gets larger as the electrons come out at more forward angles, leading to a larger energy spread of the deuterons for a given value of Q. Finally, it becomes increasingly difficult to maintain the kinematical match between the electron and the deuteron since the deuteron scattering cone spreads out. Our choice of deuteron angle was driven primarily by considering these factors at our highest proposed data point where the counting rates are smallest. After a careful study of different deuteron channel configurations, we have chosen 3.2 GeV as beam energy for $Q = 6.2$ fm^{-1}. This corresponds to a fixed deuteron scattering angle of 60.5°.

4.2 Detection of the Electron

Elastically scattered electrons in the range of 1-4 GeV/c will be detected in the HMS spectrometer. The time and energy information of the scattered electrons will be used in conjunction with the deuteron detection system to allow the rejection of background charged particles reaching the polarimeter. Because the electron and deuteron are detected in coincidence, the kinematics of the scattering process are constrained and only modest requirements on particle identification and resolution are made on the electron detector system. We have assumed a solid angle of 6 msr with a point-point focus, a target length acceptance of ±5cm (at 90°) a momentum acceptance of 5% and a momentum resolution of 10^{-3} in designing the experiment.

Information from the electron arm will also be used to determine the energy

spectrum of the scattered deuterons. This distribution allows the interpolation of the calibration data to obtain the averaged cross sections and analyzing powers used to perform the polarization measurement. The electron arm information (angle, energy of the scattered electrons) have been simulated with a Monte Carlo code taking into account multiple scattering and Bremsstralhung in the LD_2 target. The result was that this information permits the reconstruction of the energy spectrum of the deuteron with good precision ($\approx$ 2 MeV at T_d = 200 MeV and 4 MeV at T_d = 400 MeV).

The deuteron detection angle is fixed, so the electron spectrometer will be rotated to match the 2 body kinematics of the D(e, $e'\vec{d}$) reaction. The required angles are in the range of 20-37°. The distance from the target to the first quadrupole of the HMS is continuously adjustable. Therefore in actual running this distance can be selected to maximize the product of solid angle, target length acceptance, and overlap with the deuteron channel acceptance at all electron angle settings.

4.3 The Deuteron Transport Channel

4.3.1 Deuteron Channel Design

For the deuteron arm, we propose to build and install a specially designed magnetic channel, the purpose of which is both to focus the maximum number of deuterons onto the polarimeter target, and to protect the polarimeter from a direct view of the target, thereby reducing the background in the polarimeter to only high energy protons.

The latter of these two requirements is straightforwardly satisfied by incorporating a magnetic bend into the channel. The issue of background in the polarimeter is addressed in more detail in section 6. The main design considerations of the channel are driven by the first requirement. The experimental counting rate will be determined by the e-d cross section multiplied by a factor f which is the acceptance overlap between the electron and deuteron arms. To first order in φ_e and φ_d (the angles of elevation from the horizontal plane), the factor f is deduced from the acceptances of both arms and from the kinematic relations:

$$\frac{d\theta_d}{d\theta_e} = -\frac{\sin 2\theta_d}{2\sin\theta_e} \tag{4.1}$$

$$\frac{d\varphi_d}{d\varphi_e} = -\frac{\sin\theta_d}{\sin\theta_e} \tag{4.2}$$

$$\kappa \equiv \frac{1}{p_d}\frac{dp_d}{d\theta_d} = -\frac{2E_e'^2 \sin^2\theta_e}{\beta_d M_d p_d \sin 2\theta_d}. \qquad (4.3)$$

For a fixed Q^2, the beam energy can be varied to maximize the product $f\,(d\sigma/d\Omega_e)$. The cross section increases somewhat faster than E_e^2, while f, within a certain range, decreases like $1/E_e$. This is due mostly to the fact $(d\varphi_d/d\varphi_e)$ increases very rapidly with the energy, so at higher energies it becomes increasingly difficult to accept all of φ_d.

From these considerations alone, it would still be most favorable to use the highest possible beam energy for the highest kinematics setting. However, the energy spread of the deuterons incident upon the polarimeter should not exceed ± 35 MeV. Indeed an interpolation of the calibration data and an integration of the deuteron energy spectra are necessary in the extraction of t_{20} and should not be performed over too large energy domain. The binning in Q should also be limited to a reasonable value compatible with the expected variation of t_{20} (± 0.3 fm^{-1} for the largest Q point). These requirements, plus the additional increase in κ and $(d\theta_d/d\theta_e)$ with energy and the increasing contribution of second order effects in the deuteron optics, place a limit to the beam energy of 3.2 GeV at $Q = 6.2$ fm^{-1}.

The proposal to PAC 6 used a beam energy of 2.2 GeV at the maximum kinematics. Since that time, we have studied various schemes to improve upon the previous design, keeping in mind the above considerations. A perfect match ($f = 1$) with the electron arm at 3.2 GeV, 6.2 fm^{-1} would require an acceptance $\Delta\theta_d = \pm 23.5$ mrad, $\Delta\varphi_d = \pm 179$ mrad, and $\Delta p_d/p_d = \pm 5$ % (with the 12 cm target length acceptance). We tried solutions with the largest available (warm) magnets at DESY, BNL, SLAC and Saturne. The solutions requiring $f = 1$ were impractical either from the point of view of set-up (in particular the first quadrupole Q1 near the target) or of available power supplies (none of the available power supplies at CEBAF would have been sufficient). We then investigated whether it was more beneficial to reduce the target length or cut in the azimuthal angles and concluded that a reduction in φ_d was preferable.

Our proposed design (see figure 2) is now a QQ$_S$QD transport channel (the S subscript means that this quadrupole will be equipped with additional coils for sextupolar corrections). The first quadrupole Q1 is brought as close as possible to the target (this will require a new vacuum chamber) and must focus vertically because of the large spread in φ_d. Because of the target length and the vertically focusing Q1, the horizontal envelope then blows up, requiring Q2$_S$ to have a rectangular aperture. Adding a third quadrupole results in a more symmetric distribution of

deuterons on the polarimeter target. The dipole is standard and provides a 25° bend. The direction of the bend and the tune of the quadrupoles are chosen so as to compensate to first order for the kinematical variation of momentum with angle: $(x|\theta)+\kappa(x|\delta)=0$. In the vertical direction, we imposed point to point focusing from the primary target to the polarimeter target ($(y|\varphi)=0$). An adjustment around this first order tuning is necessary since second order effects are sizeable. Using again the kinematical correlation, small sextupolar fields are introduced to realize the condition $(x|\theta\delta)+\kappa(x|\delta^2)=0$ (see figure 3). Higher order effects were found negligible by comparing second order and raytrace (in ideal fields) calculations.

In this design, the vertical angle acceptance is ± 130 mrad, and the θ and δ acceptance overlaps completely with the HMS acceptance. The resulting mismatch factor f ranges from 0.92 at $Q = 4$ fm^{-1} to 0.62 at $Q = 6.2$ fm^{-1}.

The characteristics of the channel are the following (the fields and gradients are given for 400 MeV deuterons, corresponding to $Q = 6.2$ fm^{-1}):

1. Quad Q1: 10Q36 (available at CEBAF). $L_{eff} = 96.5$ cm, Grad = 8.22 T/m.

2. Quad Q2: rectangular aperture quadrupole ($\pm$ 35 cm in horizontal, $\pm$ 7 cm in vertical); a magnetic design is currently underway at Saturne (see figure 4), and will be finalized upon approval of the experiment; L_{eff} = 100.6 cm, Grad = 3.88 T/m. Additional coils will provide a small sextupolar field.

3. Quad Q3: 10Q36 (available at CEBAF). $L_{eff} = 96.5$ cm, Grad = 3.47 T/m.

4. Dipole: L_{eff} = 126 cm, B = 1.79 T, gap = 15 cm. We have located a dipole, which exceeds these specifications and with its power supply, at Bates.

Even though the optimization of the deuteron channel optics were performed for the $Q = 6.2$ fm^{-1} kinematics, *POLDER* has reasonable analyzing power up to deuteron energies of 500 MeV (corresponding to a momentum transfer of $Q =$ 6.8 fm^{-1}). Thus an additional measurement is feasible even though the mismatch factor f would decrease to $f = 0.42$. The optimization of the deuteron channel at 6.8 fm^{-1} would have led to unrealistic requirements on the magnets. Nonetheless, in ten days of running at a beam energy of 4 GeV, it would be possible to make a measurement with more modest statistics at this point. We have therefore included such a measurement in the overall beam request.

Figure 3

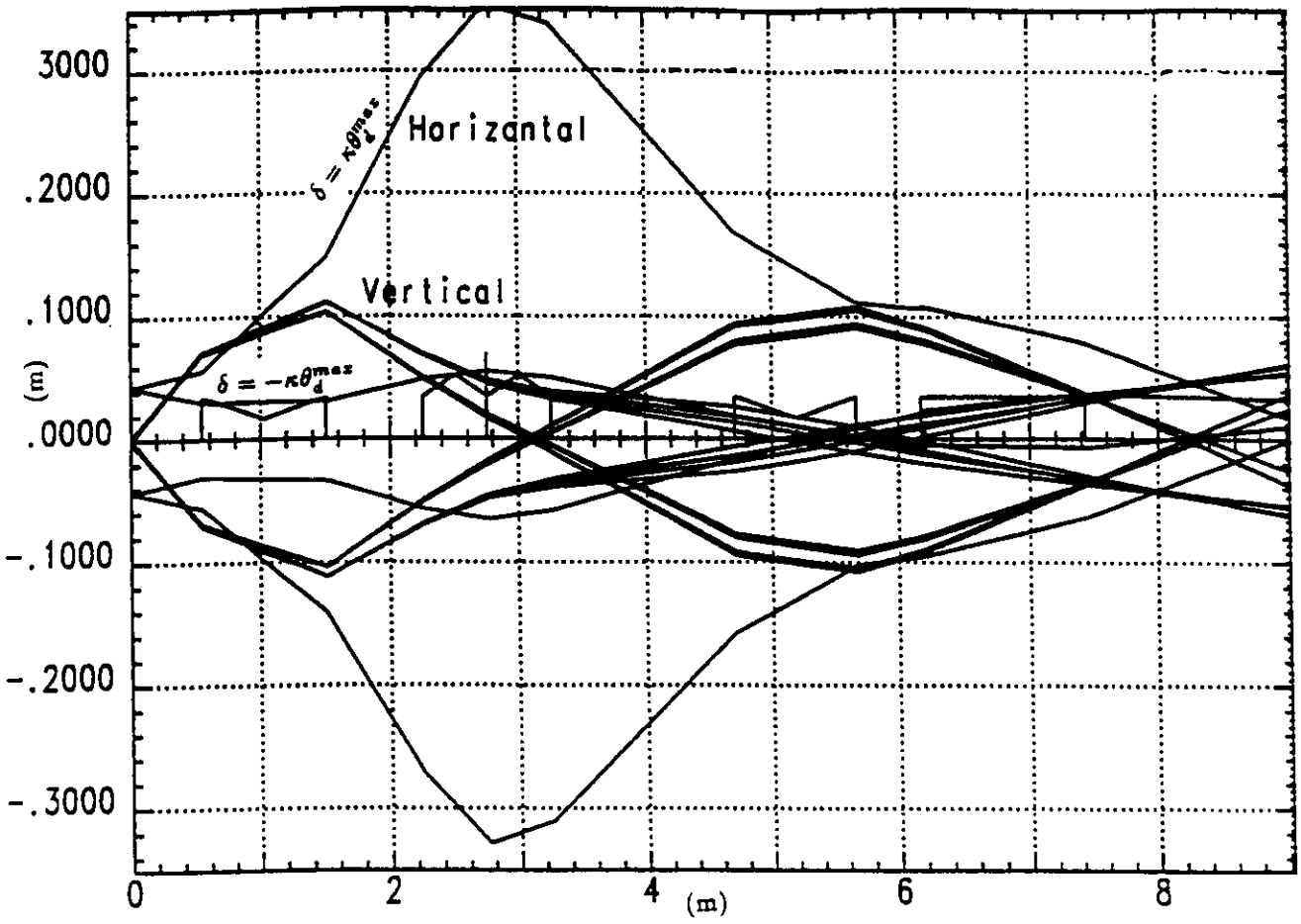
3000
.2000
.1000
.0000
-.1000
-.2000
-.3000
(m)
0
2
4
6
8
(m)
Horizontal
Vertical
$\delta = \kappa\theta_d^{max}$
$\delta = -\kappa\theta_d^{max}$

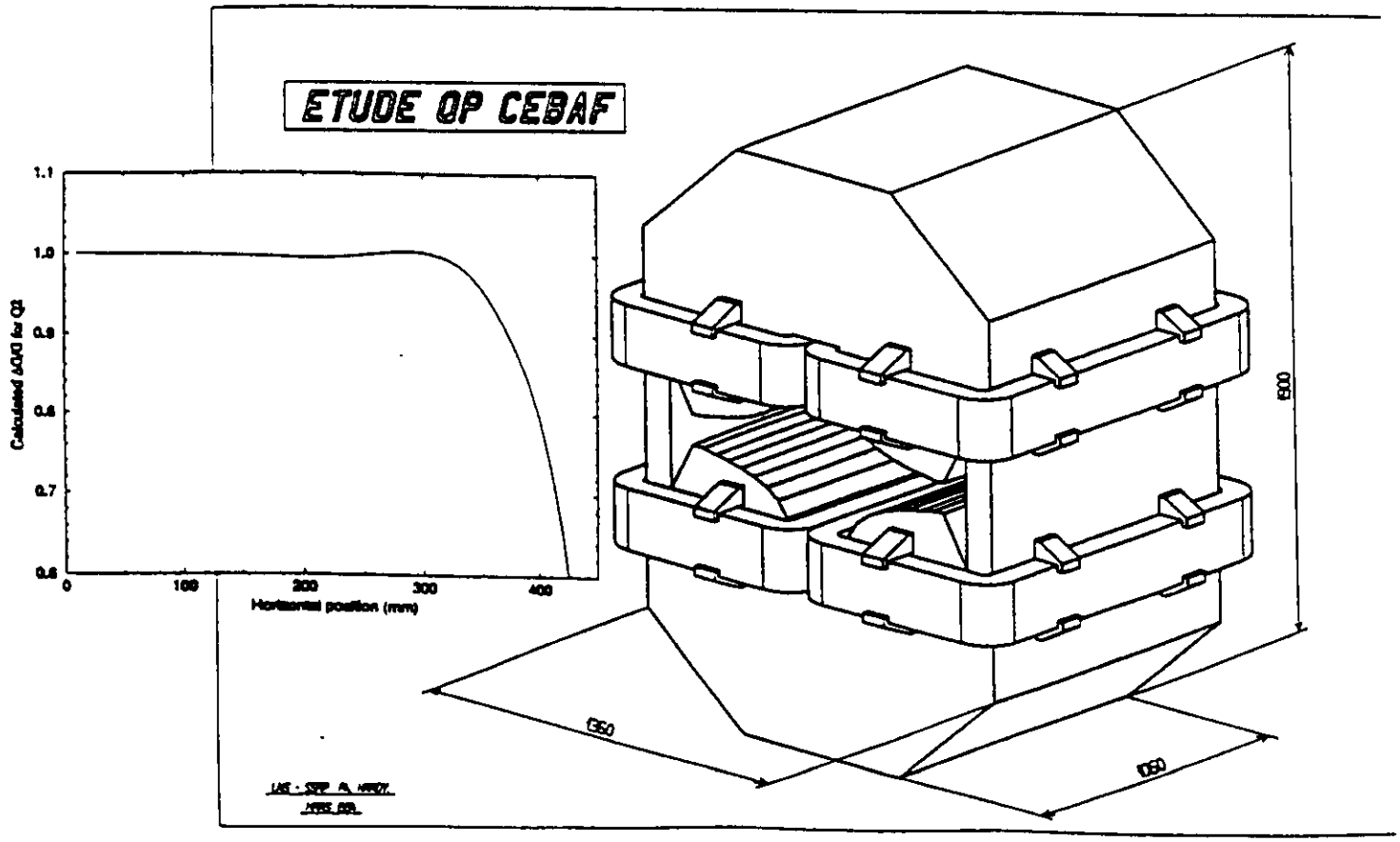
ETUDE OP CEBAF
1.1
1.0
0.9
0.8
0.7
0.6
0
100
200
300
400
Horizontal position (mm)
1500
1050
1050

4.3.2 Required Infrastructure

The magnetic elements of the deuteron channel will be provided either by the collaboration or already exist at CEBAF. However, a certain level of infrastructure will need to be provided by CEBAF in order to mount the deuteron channel on the floor of the experiment hall. Mechanical support and alignment fixtures for all magnets will be provided by the French part of the collaboration. Below is a list of the major items requested from CEBAF by the collaboration:

1. Power supplies: All magnets, except the dipole, can be powered by the existing power supplies normally assigned to the SOS spectrometer. The dipole power supply (Bates) has to be installed in Hall C with its cables and controls.

2. Electrical power: Total of about 580 kW (at 6.2 fm^{-1}).

3. Cooling water: Available from Hall C (SOS)

4. Construction of a new, smaller vacuum chamber (see the section on the LD_2 target).

5. Ordinary concrete as a base support for the whole channel (about 90 m^3) and concrete for the shielding hut surrounding the polarimeter (about 30 m^3).

6. Helium bag: Vacuum chamber walls in the magnetic elements would degrade the transmission of deuterons by at least 15%. We have therefore chosen to use helium bags through the channel. Multiple scattering from the required 8 m long helium bag would be comparable to that in the LD_2 target.

4.3.3 Simulations

Monte Carlo simulations of the deuteron channel are underway to evaluate several issues. A first order estimate of the mismatch factor, f, was generated by simulating the *e-d* cross section, accounting for beam size, energy loss in the target, electron acceptance and estimate of the deuteron phase space acceptance using first order matrix elements. The mismatch factors used for the beam time request were then estimated by raytracing correlated ($\delta_d = \kappa\theta_d$) trajectories through the channel, taking into account the finite aperture of the magnets, using the code ZGOUBI developed at Saclay. They are 10−15% smaller than the first order estimate. Another simulation is underway, in order to account for multiple scattering and nuclear reactions within materials on the deuteron path (code REVMOC, developed at TRIUMF).

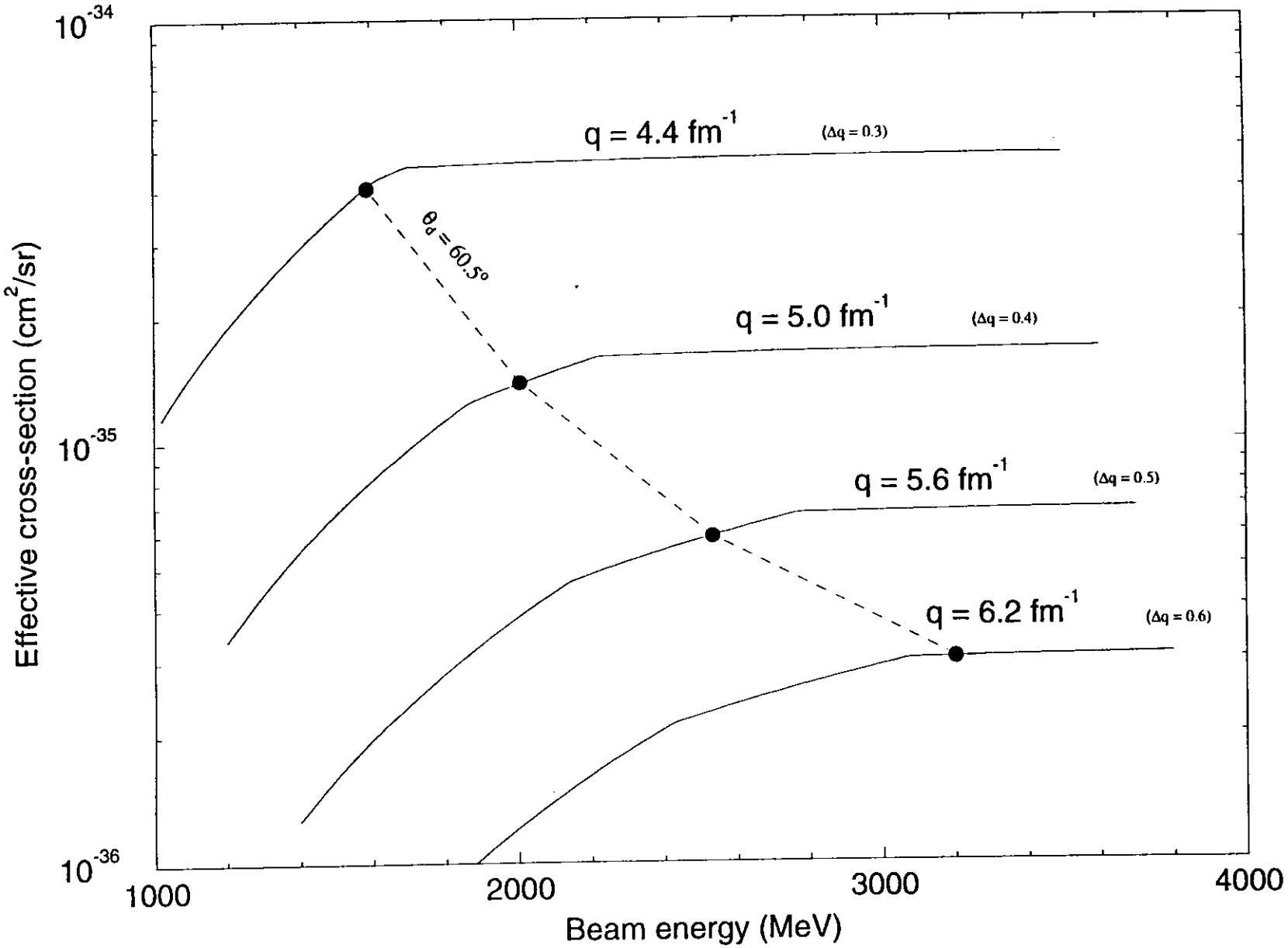
10^{-34}
10^{-35}
10^{-36}
Effective cross-section (cm^2/sr)
q = 4.4 fm^{-1} (Δq = 0.3)
θ_q = 60.5°
q = 5.0 fm^{-1} (Δq = 0.4)
q = 5.6 fm^{-1} (Δq = 0.5)
q = 6.2 fm^{-1} (Δq = 0.6)
1000
2000
3000
4000
Beam energy (MeV)

Figure 5 illustrates the variation of $f(d\sigma/d\Omega_e)$ with beam energy, for fixed values of Q. The initial rise is due to the Mott cross section (with $f = 1$), then f decreases because the deuteron channel acceptance is no longer able to match the electron solid angle. The leveling to a constant value is due to the requirements that the range of Q covered in one setting of the electron spectrometer be reasonable and, for the highest Q points only, that the maximum deuteron energy spread at the polarimeter not exceed ± 35 MeV.

In addition to simulation of the acceptance for deuterons, the transmission of background protons was simulated using the first order transport matrix elements. This point will be discussed in more detail in section 6.

4.4 The LD_2 Target

With a beam intensity of 100 μA, the availability of a high power LD_2 target is crucial for this experiment. With a 12 cm target cell, approximately 400 watts of beam power will be deposited in the target. The "standard" Hall C cryogenic system is designed to run at a maximum power deposition of only 200 watts, which will not be adequate for this experiment. However, we plan to upgrade the target by a factor of 2 with some relatively straightforward modifications. It is currently thought that the limitation in target power capacity will most likely be due to the circulating fans in the target loop, which presently are commercial fans, readily available but not necessarily optimized for maximum throughput. In addition, the design value of 200 watts assumes 50% efficiency of the fans, whereas the true efficiency has not yet been measured. Studies are currently underway at CEBAF to determine the actual performance of the fans. If either improvement in the fan design or a totally new target design is required, the collaboration is prepared to provide a specialized target for the experiment. Another important feature regarding cryogenic power is that this experiment does not depend on absolute cross section measurements of the primary e-d scattering. Thus one can accomodate small local changes ($\leq$ 10%) in density of the LD_2 target, which simplifies greatly the issue of cooling. Finally the beam on target will also be rastered in order to help avoid local boiling.

We have estimated the rates of both deuteron and proton background coming from the aluminum windows, which represent a small fraction of the total target thickness. The results show that these contributions are small compared to the rates induced in the LD_2 and thus the target will not be collimated on either the deuteron or electron side. The overall useful target length will be about 10 cm. In

order to attain the high degree of kinematical matching, a small scattering chamber will be required. This has been discussed with the Hall C staff and appears to be feasible if only a single recirculation loop is used in the target system.

5 Polarization Measurement

One key element of the experiment is the polarimeter which measures the polarization of the recoiling deuteron.

A polarimeter requires a nuclear reaction to have both large analyzing powers and cross sections in order to yield measurable asymmetries with respect to the incident particle polarizations. The cross section for such a reaction depends upon the incident polarization through [35] :

$$\sigma(\theta,\phi) = \sigma_0(\theta)\ [1 + t_{20}\ T_{20} + 2\,(it_{11}\,iT_{11} + t_{21}\ T_{21})\,cos\phi + 2t_{22}\ T_{22}\ cos2\phi] \quad (5.1)$$

where T_{kq} are the analyzing powers of the reaction, t_{kq} the polarization coefficients of the particles and σ_0 the cross section for unpolarized incident deuterons. Here ϕ is the angle between the normals to the polarimeter reaction and the *e-d* scattering planes.

Unpolarized cross sections and analyzing powers (σ_0 and T_{kq}) have first to be measured in calibration runs with beams of known polarization. With them, the polarimeter can then be used to deduce the polarization of incident particles from experimental asymmetries.

Polarimeters are characterized by a so-called figure of merit given by

$$(F_{kq})^2 = \int (T_{kq})^2\ \epsilon(\Omega)\ d\Omega \quad (5.2)$$

where ϵ is the ratio of the number of reactions to the number of incident particles ($N_{incident}$) and T_{kq} the analyzing powers of the reaction. These quantities are integrated over the phase space covered by the polarimeter. The figure of merit allows one to compare different competing type of apparatus because it governs the statistical error made in a polarization measurement through the following relation :

$$\Delta t_{kq} = \frac{1}{\sqrt{2-\delta_{q0}}} \left(F_{kq}\sqrt{N_{incident}}\right)^{-1} \quad (5.3)$$

From this, one sees that the larger the figure of merit, the smaller the error for a given number of incident particles (and thus of beam time).

5.1 The *POLDER* Polarimeter

POLDER is based on the ^{1}H($\vec{d}$,2p)n reaction as proposed by Bugg and Wilkin [36]. At 200 MeV the measured figures of merit (F_{20} and F_{22}) in the ^{1}H($\vec{d}$,2p)n [37] reaction were found to be comparable to those of the ^{1}H($\vec{d}$,p)X reaction used in the *AHEAD* polarimeter [11]. However the crucial feature of the ^{1}H($\vec{d}$,2p)n reaction is that its figures of merit remain large up to at least 500 MeV [37] whereas those of the ^{1}H($\vec{d}$,p)X reaction fall quickly above 200 MeV [38]. The figure of merit F_{11} for the vector analyzing power is zero for this reaction. Also the ^{1}H($\vec{d}$,2p)n reaction is well understood in terms of the impulse approximation [39], and theoretical predictions can thus be used for numerical simulations.

The experimental setup is shown in figure 6. The directions and impact points of incident deuterons on the target are measured with good precision by two multiwire proportional chambers (MWPC1/2) placed upstream of the target. New chambers with 3 wire planes each have been developed for CEBAF and should provide $\sim$ 100% efficiency per chamber. They are also capable of detecting multi-hit events with good precision, thus permitting the rejection of events with two charged incident particles. At CEBAF this will be used to reject the proton background remaining after the deuteron channel.

The measurement of the number of deuterons incident on the target, necessary for cross section normalization, is determined by a coincidence in two detectors (S1 and S2) composed of thin fast plastic scintillators optically coupled to two phototubes. The coincidence signal from these two detectors is part of the hardware trigger and is also used as the start signal for the time-of-flight measurement of the protons produced in the reaction. The total dead time of the experiment vetoes this coincidence and so exactly the same correction is applied to the measured number of reactions and incident deuterons. The information provided by the electron spectrometer in coincidence with *POLDER* will ensure the the rejection of the background particles reaching *POLDER*. Finally, the analog signal of the start detector will be recorded to permit additional discrimination between deuterons and background protons of the same momentum.

The ^{1}H($\vec{d}$,2p)n reaction takes place in a liquid hydrogen (LH_2) target of cylindrical shape, 16 cm long and 10.2 cm in diameter. The target cell is made of 170 μm thick mylar with an entrance window of 120 μm thick kapton. It is mounted in a vacuum chamber with entrance and exit windows made of titanium 50 and 100 μm thick, respectively. The target is operated at a temperature of 19 K, controlled by a

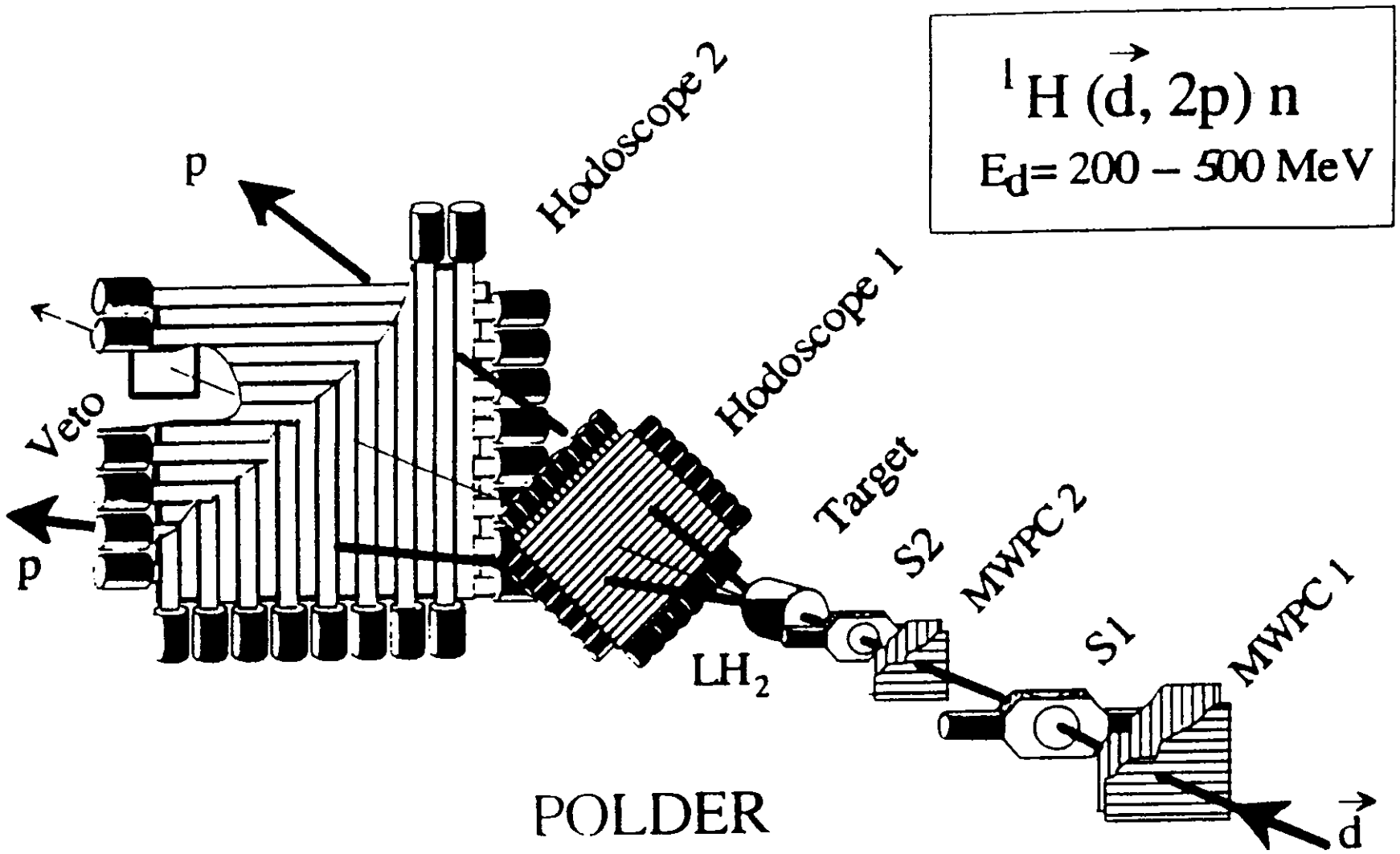
$^1H(\vec{d}, 2p)n$
E_d= 200 – 500 MeV
p
Hodoscope 2
Hodoscope 1
Veto
p
Target
S2
MWPC 2
S1
MWPC 1
LH_2
$\vec{d}$

POLDER

monitoring system, with a 10 W cryogenic system. Changes are anticipated in order to comply with the US safety regulations for enclosed liquid target operation as well as an increase of the target cell dimensions (to reach 14 cm in diameter and 20 cm in length).

The protons created in the ^{1}H($\vec{d}$,2p)n reaction are detected in two hodoscopes placed after the target, as shown in figure 6. The solid angles covered by these hodoscopes permit the detection of protons with good efficiency from the ^{1}H($\vec{d}$,2p)n reaction in the range of momentum transfer to the neutron (q) where most of the cross section of the ^{1}H($\vec{d}$,2p)n reaction is located. The hodoscopes consist of two planes providing X and Y information. The scintillator thicknesses (0.2 cm and 1 cm for the first and second hodoscopes) are small in order to reduce the $(d, 2p)$ reaction rate in the detectors. Dead areas have been minimized and the detection efficiency for $(d, 2p)$ events is about 90%. The plastic bars are optically coupled to a phototube at only one extremity. The information on the numbers of the bars fired in the two hodoscopes permits one to determine the directions of the protons. To achieve this, the first hodoscope is rotated by 45°. At our energies, the characteristics and kinematics of the ^{1}H($\vec{d}$,2p)n reaction allow one to discriminate charge exchange events from other parasitic reactions by the simple condition that **two charged particles** are detected at velocities close to those of the incident beam. As the thin plastic scintillators making up *POLDER* are mostly sensitive to charged particles, no particle identification is necessary. The velocity of the detected particles is obtained by a time of flight measurement and energy measurements are therefore not necessary. These features greatly simplify the operation of the apparatus. In addition, since **only** logic signals are used in the $(d, 2p)$ cross section determination, the calibration should be preserved in transporting the polarimeter from Saturne to CEBAF.

Finally, a veto detector is placed on the beam axis. This detector is composed of an absorber which stops the protons of interest and of a plastic scintillator coupled to two phototubes which detects the deuterons and background protons reaching the polarimeter. This veto detector allows one to reject background events associated with the detection of at least one incident deuteron or one fast proton.

The mechanical positioning for all the elements of the setup is made with good accuracy. In particular, the relative distances of these elements will be retained when transporting *POLDER* from one location to another An off-line procedure, which is based on data from the two MWPC's upstream of the target and a third after

the second hodoscope, is also used to determine precisely the relative alignment of the MWPC and hodoscopes. This alignment uncertainty mostly influences the t_{21} determination, and leads to a systematic error of less than 0.03 for this quantity.

The connection of the electronics of *POLDER* to the electron arm detectors is under study. The expected acquisition rate (a few events per second) can be handled easily. An Ethernet link may be used to send data to a dedicated workstation for on-line control and sophisticated event selection. During the calibration runs, preliminary deuteron polarizations were obtained in a few days using this procedure.

5.2 Calibration of the Polarimeter

The polarimeter was calibrated in 1992 and 1993 for incident deuteron energies ranging between 175 and 500 MeV [10]. Additional cross section measurements will be performed at Saturne in 1995 to have calibration data points every 25 MeV (instead of 50 MeV for the time being) and also to check the changes induced by having longer (20 cm instead of 16 cm) LH_2 target for the polarimeter. Since *POLDER* can be easily transported and mounted, cross check calibration runs could be performed (at IUCF for example) after the t_{20} measurement if necessary.

The calibration experiments were performed using the polarized deuteron beams delivered by the Saturne synchrotron which can provide deuterons of known vector and tensor polarization (with a 2−3% accuracy [40]). *POLDER* was installed in the focal plane of the spectrometer SPES1. In order to measure the T_{21} analyzing power, a superconducting solenoid was used to in conjunction with the SPES1 spectrometer acting as a dipole magnet. For consistency checks, some measurements were performed both with and without the solenoid.

5.2.1 Data Handling and Background Rejection

The selection of the *pp* pairs originating from the $^1H(\vec{d},2p)n$ reaction is performed using a limited number of gates. Background events, which reduce the polarization signal and contribute to the cross section in a non-reproducible way, are rejected in the data analysis using cuts on the time-of-flight information of the detected particles and from the information provided by the wire chambers and the veto detector.

Accurate time-of-flight data ($\leq$ 1 ns FWHM) are obtained after corrections for the transit time of light in the bars. As the two protons created in the $^1H(\vec{d},2p)n$ reaction have very similar velocities, another gate can be set on the difference in their corrected times of flight.

The two wire chambers placed upstream of the target detect the incident particles and measure their direction. This information is also obtained for multi-hit events and, based on simple multiplicity criteria, events with more than one incident particle can be rejected. This was necessary during the calibration run as events with two deuterons simulated the $(d, 2p)$ reaction with two charged particles in the hodoscope.

The direction of the two protons is fixed by the number of the bars which fire in the two hodoscope. From these and the MWPC information one can determine the direction of the center-of-mass of the pp pair and thus its polar angle θ (closely related to the momentum transfer q to the neutron) as well as its azimuthal angle ϕ. Since large tensor signals are only found for small excitation energies of the pp pair ($E_x \leq 8$ MeV) [37], this quantity is derived from our data by using the relative angles of the two protons. The calculated E_x differs slightly ($\approx$1 MeV) from the exact one, but it provides very stable cross section values when cuts are applied.

Using the directions of the incident deuteron and those of the two protons, the vertex of the reaction is reconstructed by a fitting procedure. This permits us to cleanly discriminate between events originating from the target and those created elsewhere (mostly the plastic bars of the first hodoscope). Typical precision of a few centimeters for the z coordinate, and a few millimeters for x and y, are obtained.

Calibration data treated in this fashion were compared with the results of a simulation program which uses impulse approximation predictions [39] filtered by the same experimental cuts. Figure 7 shows the excellent agreement between data measured at ($T_d = 300$ MeV) and the simulation, for key quantities of our experiment (the excitation energy of the pp pair E_x, the momentum transfer q, the z component of the vertex and the difference of time of flight). Since the theory has been previously checked with a different detector [37], this result gives us confidence in the data handling and background rejection.

5.2.2 Analyzing Power and Cross Section Determination

Counting rates for the ^{1}H($\vec{d}$,2p)n reaction events, binned in q and ϕ, are measured for different beam polarizations and combined, for the same number of deuterons, to construct vector and tensor asymmetries. The sum of these normalized yields provides the counting rate for an unpolarized beam. The analyzing powers (T_{kq}), which are related to the asymmetries, are determined using a χ^2 minimization procedure.

For our t_{20} experiment, absolute values of the unpolarized cross sections must be very well known and thus many different experimental conditions have been tested.

EXPERIMENT and SIMULATION 300 MeV

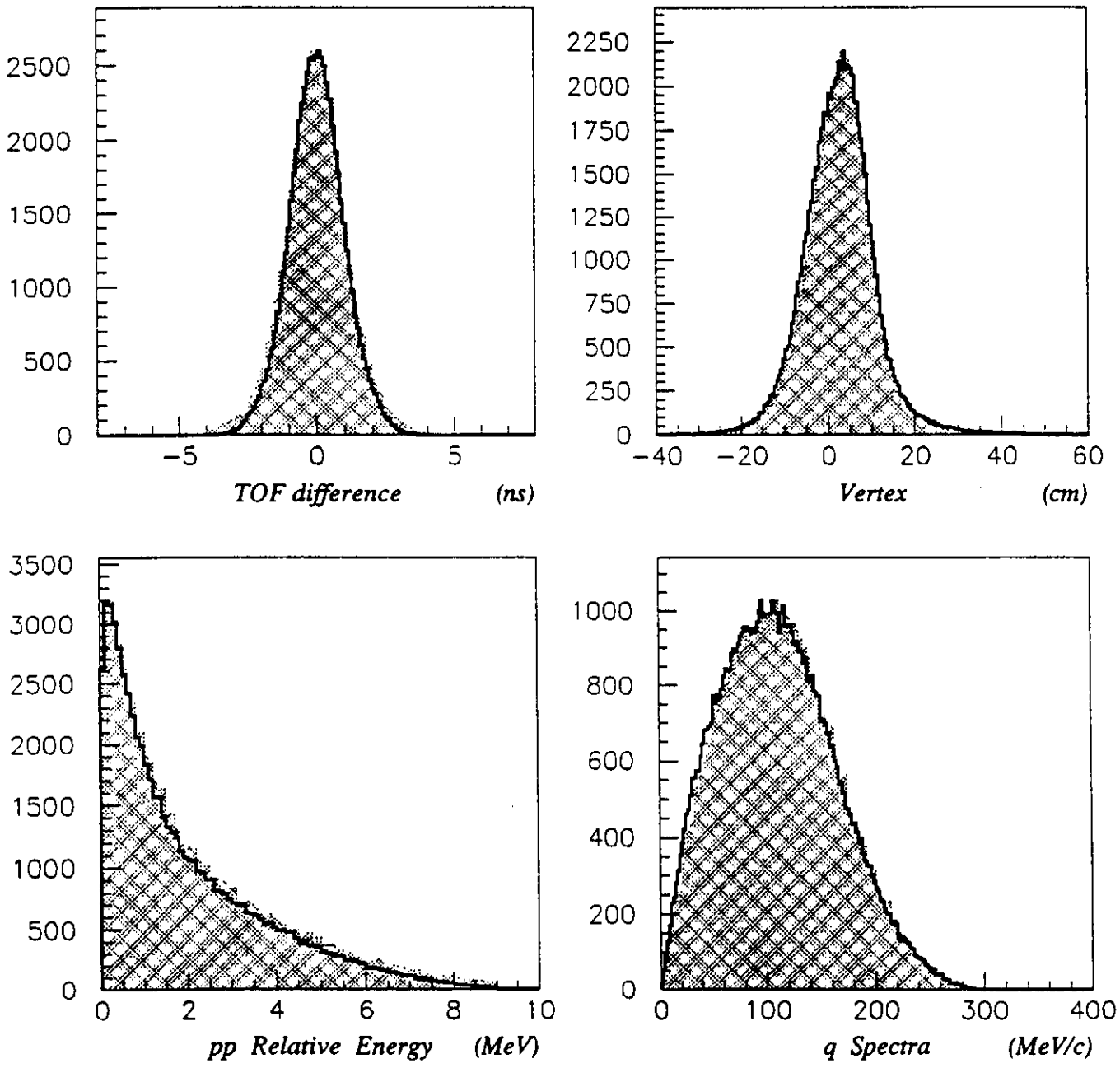

figure 7

In particular, the dependence on the beam intensity and direction was examined. The unpolarized cross section deduced from these measurements in different runs, after all off-line cuts, were stable and mutually compatible within statistical errors as illustrated in figure 8. Systematic errors were estimated to be less than 0.5% for the unpolarized cross section in our setup and data treatment.

The results obtained at T_d = 200 and 400 MeV for a cut of 5 MeV on E_x are shown in figure 9. The statistical errors and the uncertainties due to the beam polarization measurement (estimated to be less than 3%) are included. The experimental cross sections have not been corrected for geometrical detection efficiencies in the hodoscopes; the rapid fall above 250 MeV/c indicates an increasing effect occurring in *POLDER* at large detection angles. In figure 9, the tensor signals exhibit a very smooth dependence with q and typical statistical errors of better than 5% were obtained at 120 MeV/c. The vector analyzing power (iT_{11}) is consistent with zero as expected in the impulse approximation model. The T_{21} values are somewhat larger than expected. The cross sections become higher as the beam energy decreases, leading to larger figures of merit. A calibration data set is now measured between 175 and 500 MeV.

The integrated figures of merit are shown for all tensor signals and for four beam energies in figure 10. These figures of merit F_{kq} are displayed as a function of the upper cut in E_x set on the data.

5.3 Deuteron Polarization Measurements

Knowing the unpolarized cross section and analyzing powers (T_{kq}) of the ^{1}H($\vec{d}$,2p)n reaction from calibration runs, the asymmetries in counting rates allow one to determine the incident particle polarization tensors. The experimental asymmetries measured in *POLDER* are given by:

$$\begin{aligned} N(q,\phi) = \; & kN_0(q)(1 + 2it_{11}\, iT_{11}(q)cos\phi + t_{20}\, T_{20}(q) \\ & +2\; t_{21}\, T_{21}(q)cos\phi + 2\; t_{22}T_{22}(q)cos2\phi) \end{aligned} \tag{5.4}$$

A χ^2 minimization procedure is used to calculate the polarization tensors of the deuterons (t_{kq}) from the q (θ), and ϕ dependence of this cross section. All geometrical and detection efficiencies are in principle contained in the unpolarized cross section measured during the calibration run, but an overall normalizing factor k may be needed. However, the strong correlation between the values of the cross section and

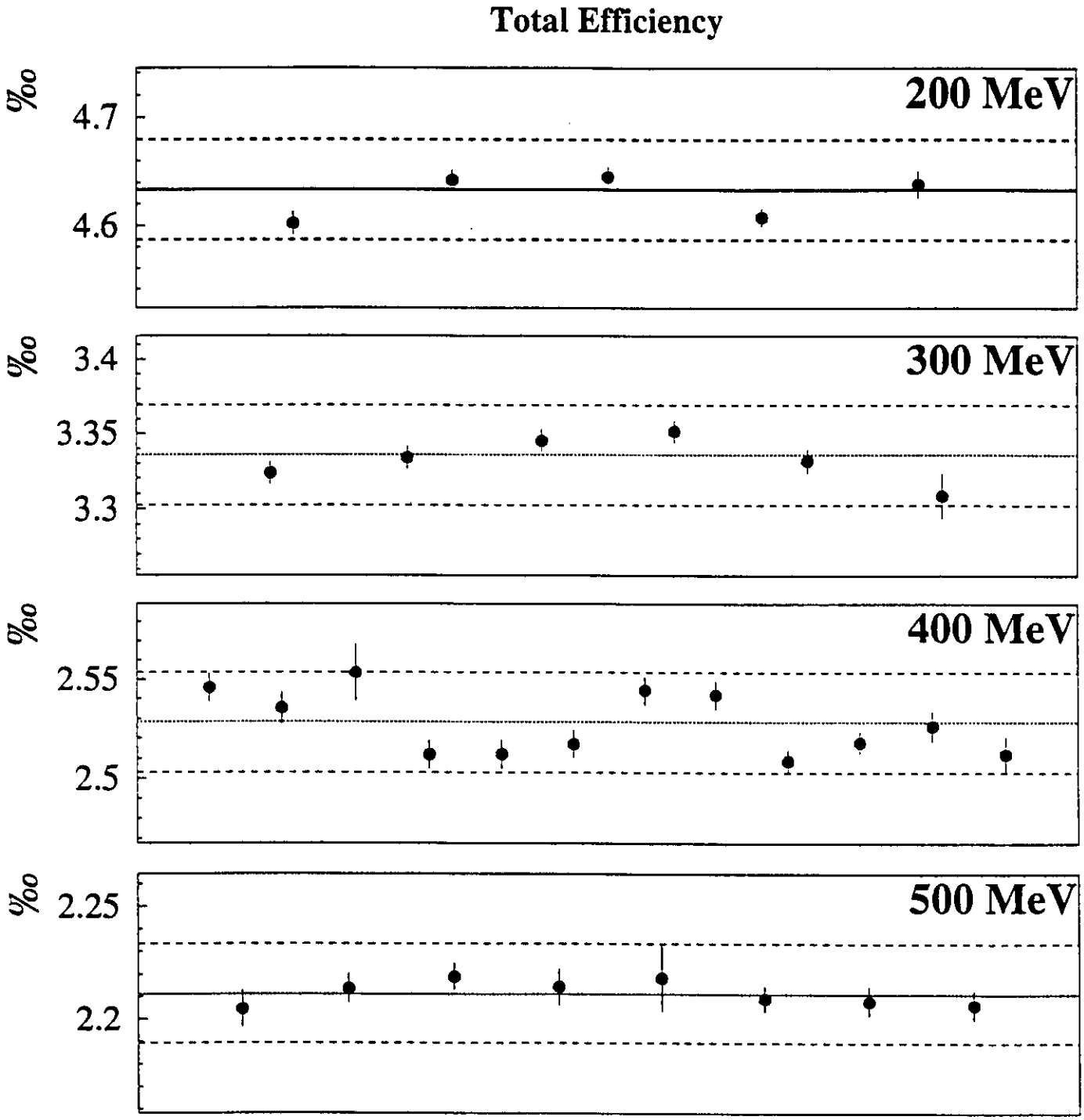
Total Efficiency
‰
4.7
4.6
200 MeV
‰
3.4
3.35
3.3
300 MeV
‰
2.55
2.5
400 MeV
‰
2.25
2.2
500 MeV

Figure 8

t_{20}, leads to large systematic errors if k is left completely free:

$$\Delta t_{20} \approx \frac{1}{\Delta k \times T_{20}} \tag{5.5}$$

This is far less important for t_{22} and t_{21}, which are defined mainly by their ϕ dependence. The calibration runs have shown that the unpolarized cross section measurement can be controlled at a level better than 1%, allowing one to fix k to within 1 % in the fitting procedure. With the average T_{20} at ~ 0.2, the typical systematic errors are about 0.05 and will be added to the statistical error of the polarization measurement.

Data recorded during the calibration run has been analyzed following the procedure described above to check the ability of *POLDER* to be operated in polarimeter mode. Errors associated with the recorded statistics were studied during the calibration and polarization measurement runs, and with the fitting procedure. The polarizations extracted from the fitting procedure were compared with those measured after the deuteron source at low energy by the means of a polarimeter The beam polarization measured at low energy is given with its associated statistical error. All three tensor polarization (t_{20}, t_{21}, t_{22}), results agreed within the error bars as shown in table 5.1. The polarizations measured with *POLDER* for three different statistics are given with their different errors. The first errors in the table are associated with the statistics recorded during the calibration run. The second error is the statistical error of the polarization measurement and given by relation 5.5. The third errors in table 5.1 are systematic, and depend on the polarization tensor involved. For t_{20} the error is linked to the correlation between k and t_{20}, for t_{21} and t_{22} it is associated with the alignment uncertainty. The systematic errors tend to increase when $\leq 10^6$ incident deuterons are used.

figure 9

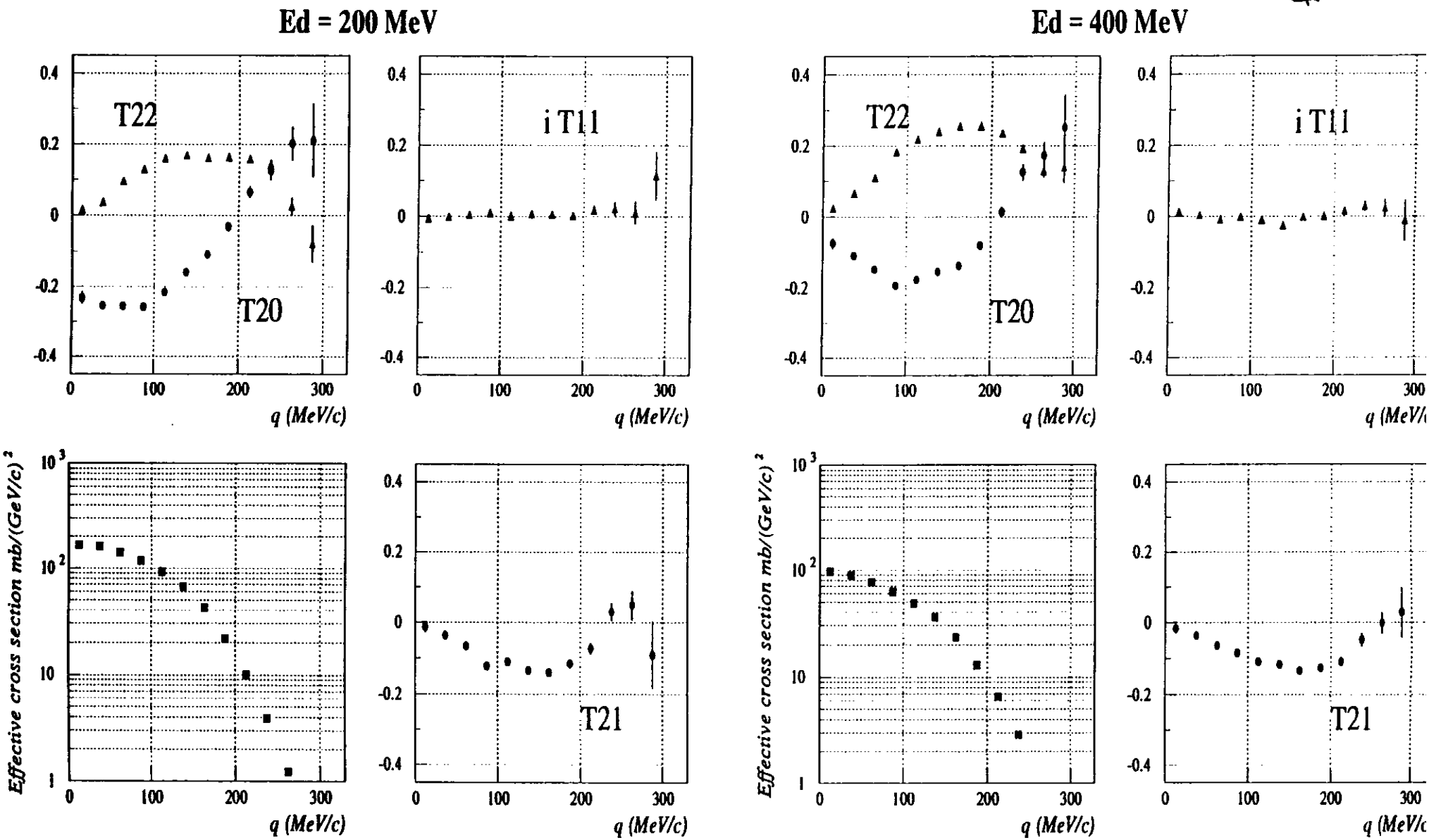
Ed = 200 MeV
Ed = 400 MeV
T22
T20
i T11
T21
Effective cross section mb/(GeV/c)²
q (MeV/c)

Figures of merit

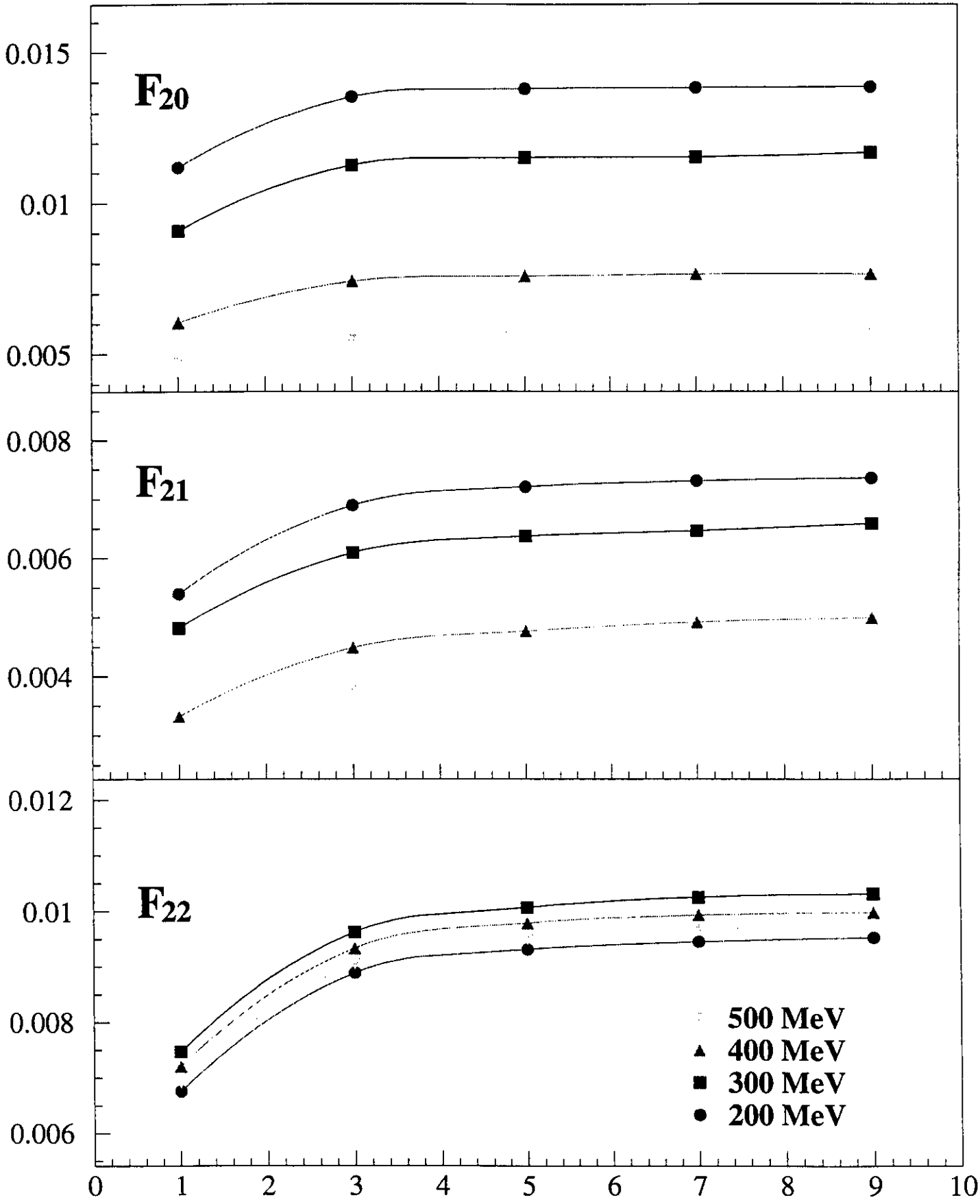

figure 10

Table 5.1

Beam polarization measured at T_d=400 MeV with *POLDER* (see text). The calibration runs have been performed with 10^9 incident deuterons.

Polarization tensors	Polarization measured at low energy	Number of deuterons	Polarization measured with *POLDER*
t_{20}	0.24 ± 0.008	4×10^7	0.24 ± 0.025 ± 0.025 ± 0.05
		5×10^6	0.28 ± 0.025 ± 0.07 ± 0.05
		5×10^5	0.33 ± 0.025 ± 0.22 ± 0.05
t_{21}	-0.22 ± 0.008	4×10^7	-0.18 ± 0.02 ± 0.03 ± 0.03
		5×10^6	-0.17 ± 0.02 ± 0.08 ± 0.03
		5×10^5	-0.27 ± 0.02 ± 0.25 ± 0.03
t_{22}	-0.355 ± 0.015	4×10^7	-0.39 ± 0.015 ± 0.015 ± 0.02
		5×10^6	-0.35 ± 0.015 ± 0.04 ± 0.02
		5×10^5	-0.23 ± 0.015 ± 0.13 ± 0.02

POLDER was also used to measure signatures of isoscalar spin-flip transitions in $A(\vec{d},\vec{d}')A^*$ scattering [10]. This is a very meaningful test of the polarimeter as the experiment was performed under severe background conditions (rates larger than 10^5 s^{-1} in the hodoscopes with 40% duty cycle). The ratio of recorded background to charge exchange events ranged from 6:1 to 30:1 and no veto detector was available. Even in these conditions, which are worse than those expected at CEBAF, the results obtained are in good agreement with expected theoretical (elastic scattering) or previously measured (inelastic) values. In particular for elastic scattering on ^{40}Ca, the results agreed with time reversal invariance. Finally, null combinations testing some systematic errors in the polarization measurement were found to be zero at the 1 % level.

6 Estimate of Background Rates

Background particles which could complicate the extraction of deuteron polarization fall into two categories. Low energy background which is removed by the magnetic channel could penetrate the concrete shielding surrounding the polarimeter and cause spurious triggers. Charged particle backgrounds of this type are predominantly generated by high energy neutrons and are discussed in more detail below. With an adequate shielding, the neutron fluxes can be kept to a reasonable level and they will not likely generate events which could simulate an *e-d* coincidence followed by two protons.

6.1 Particles Passing through the Polarimeter Shielding

The most complete study of background versus shielding for CEBAF experimental areas had been carried out for the Hall A spectrometers. Extensive evaluations of different contributions to the background counting rate were presented in two technical notes [41, 42], and are summarized here since they will represent a reasonable estimate for backgrounds in Hall C. As soon as beam becomes available in Hall C, it will be useful to make some simple measurements to check the results of these calculations.

The first consideration is background originating from direct line of sight of the target. The report used luminosity conditions of 200 μA of a 4 GeV beam on 15 cm of ^{4}He (0.17 g/cm^2) [41], into a detector placed at 12° from the beam line. The pion spectrum was calculated using the code EPRODT2 and includes electroproduction and bremsstrahlung induced photoproduction. Protons and neutrons produced by electroproduction were simulated with the code EPC of O'Connell and Lightbody [43]. The code FLUKA was used to generate the secondary particle flux created by interaction with the different shielding materials for the detector hut and between the target and the detector hut. Only high energy neutrons were studied in this part of the simulation; neutrons below 50 MeV were considered separately. With 140 cm of iron shielding, the particle flux in a 1 m^2 area at the polarimeter detector was estimated to be about 1−2 kHz. This estimate is quite conservative for our purposes because of the increased luminosity and small scattering angle considered here relative to our experimental configuration.

The second contribution to background which has been considered comes from low energy neutrons. The calculations were done for $E_n < 20$ MeV, for the Hall A detector hut [41]. The estimate is based on calculated neutron spectra with a transport to a detector inside a shielding hut. The neutron rate in the room was estimated from energy loss in the primary target (8 Watts), the 26 m long He bag (4 W), the multiple scattering in the beam dump pipe (11 W) and the beam dump backshine (11 W). The total 34 Watts were converted to a neutron flux, 4.4×10^{10} n/sec, using an empirical result from SLAC for electrons on aluminium. The shape of the neutron spectrum was assumed to have two components: a 'direct' spectrum from the interaction points which are in direct view of the shielding, and an evaporative part. The monte carlo code MCNP from LAMPF was used to simulate transport of the neutrons through the shielding. Neutron fluxes inside the hut were then estimated for different wall thicknesses. With 1 m of ordinary concrete, the

neutron flux was about $4\times10^3/s/m^{-2}$. Only a small fraction of these would actually interact in the polarimeter hodoscopes. In conclusion, the rates from neutron room background can be kept small with a reasonable shielding configuration of available concrete blocks.

6.2 Charged Particles in the Deuteron Channel

A more serious source of background for the polarimeter is charged particles which have the same momentum as the deuterons and come directly through the magnetic channel. Because of the constrained elastic kinematics and the relatively high deuteron momentum it is kinematically not possible to generate charged particles (e.g., π^+ or p) of the same momentum as the deuterons from nucleon resonance processes, even at the edges of the channel acceptance. Thus the dominant source of high energy background comes from protons from deuteron photodisintegration. This process has been modeled using $d(\gamma,p)n$ cross sections [43, 44, 45], folded with an effective virtual photon spectrum given by Wright and Tiator [46] [2]. The spectrum of incident protons was then transported through the deuteron channel. Figure 11 shows momentum and horizontal position spectra of protons incident on the polarimeter target at the lowest and highest proposed kinematics. Singles rates were calculated by integrating these spectra over the deuteron channel acceptance, and assuming a 100 μA beam incident on a 10 cm LD_2 target. The rates for each data point are listed in table 6.1. They are significant only at the lowest energy data points, and the rates will be roughly evenly distributed about the polarimeter elements upstream of the LH_2 target. It appears that they will be sufficiently small not to cause unduly high raw trigger rates in either the upstream MWPCs ($\leq$ few kHz/wire) or the polarimeter scintillators. The requirement of an electron in coincidence will reduce the accidental coincidence triggers to a low level.

If the raw singles rates were to be significantly higher than expected at the lowest beam energies, the beam current at these two data points could easily be reduced with only a small increase in total running time because the elastic e-d rate is also high at these kinematics.

The design of the deuteron channel is such that the acceptance in momentum and scattering angle is somewhat larger than required by the electron arm. Thus the channel acceptance for single protons is higher than for coincident deuterons. The rates in table 6.1 assume no collimation in scattering angle.

[2] A modified version of the (e, N) code of Lightbody and O'Connell was used to estimate rates.

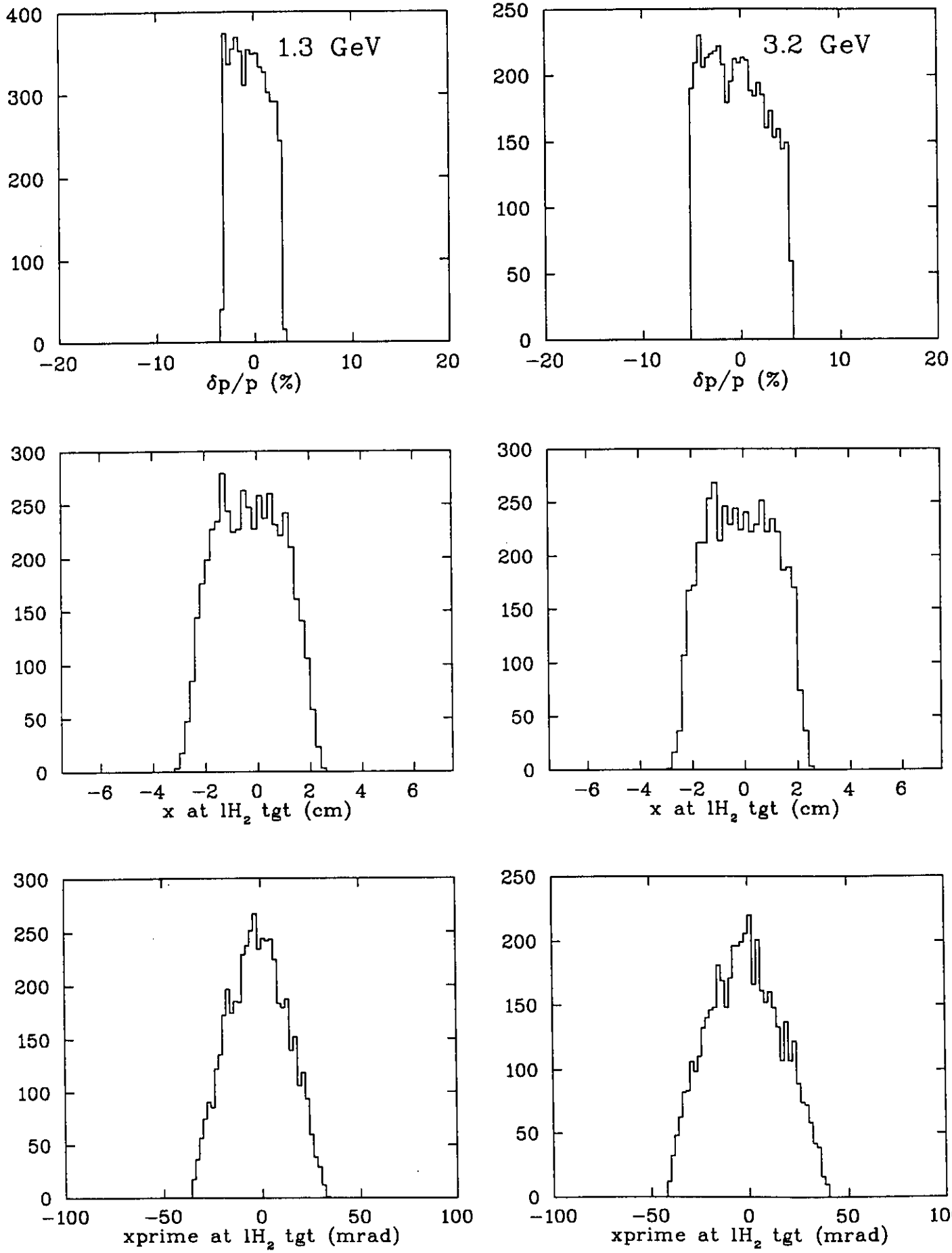
1.3 GeV
δp/p (%)
3.2 GeV
δp/p (%)
x at 1H2 tgt (cm)
x at 1H2 tgt (cm)
xprime at 1H2 tgt (mrad)
xprime at 1H2 tgt (mrad)

figure 11

Electron singles rates were also estimated, assuming that some inelastically scattered electrons will also trigger the HMS focal plane. Several different models were used to estimate the number of inelastic events incident on the lower 5% of the focal plane momentum acceptance. Because there will be no target collimation on the electron side, a 10 cm target was used to estimate electron singles rates.

The ratio of inelastic to elastic events is 3:1 at the lowest kinematics and 20:1 at the highest kinematics, leading to raw trigger rates of no more than several hundred Hz in the worst case. As on the deuteron side, triggers from charged pions are kinematically forbidden except possibly coming from the target windows, and should therefore be quite low. The last column in table 6.1 shows the overall estimated accidental coincidence rate due to electron and proton singles. The random *e-d* coincidence rate should be significantly lower.

Once it is determined that the raw proton rates are at a reasonable level, there is still the question whether these protons can be misidentified as coming from a charge exchange event in the polarimeter target. This question is addressed in detail in the next section.

Table 6.1

Estimated singles and accidental coincidence rates due to inelastically scattered electrons and protons in the deuteron channel. The following parameters were assumed: $I_e = 100\ \mu$A, Length(LD_2) = 12 cm, $\theta_d = 60.5°$, and a time window of 100 ns. For comparison, the deuteron rate from elastic *e-d* scattering is also shown (using a 10 cm useful length for the LD_2 target and including reduction factors due to kinematical mismatch and radiative losses).

T_d (MeV)	E_e (GeV)	θ_e	R_d (Hz)	R_p (Hz)	$e\ R_{inel}/R_e l$	Acc. (e,p) (Hz)
160	1.31	36.9	100	9×10^4	3	4
200	1.58	34.1	50	5×10^4	4	2
260	2.01	30.5	16	2×10^4	5	0.5
330	2.56	26.9	7	1×10^4	10	0.1
400	3.20	23.6	4	3×10^3	20	0.04
480	4.0	20.5	1.6	1×10^3	20	0.01

6.3 Rejection in *POLDER*

From the above study of various sources of background, the most important contribution will be protons having the same momentum as the deuterons of interest

and coming through the deuteron channel. Other contributions were shown to be small (some 10^3 /s/m^2) when using appropriate shielding (see previous section).

The capability of the polarimeter to identify and reject the events generated by these background protons is an important issue that we will discuss in this section.

Singles rates in the deuteron and electron arms given in the preceding section have been used as input to a simulation code generating background events which are analyzed in the same way as $(d, 2p)$ events. Three classes of parasitic events are considered in the following:

- pp accidental coincidences: the high flux of protons produces a significant number of pp coincidences. However a hardware coincidence of 100 nsec with the electron spectrometer reduces the rates of these events by a factor greater than 10^4.

- dp accidental coincidences: single protons arriving in time with real e-d coincidences will not be rejected, so no reduction factor applies from the coincidence with the electron spectrometer. This contribution will be the dominant background rate.

- p coincidence with two protons of the $(d, 2p)$ reaction: this type of trigger doesn't create an event, but the treatment of the charge-exchange (CE) event becomes more complicated, because the TDC information of the protons of interest can be affected and the information associated with the background proton should be eliminated. These events are expected to be very rare.

There are essentially three different ways to reject the background events during the data analysis. First is the time of flight information (TOF) between the deuteron start detectors and the polarimeter hodoscopes. Figure 12 presents a typical singles distribution of TOF expected in one central bar of the hodoscope where the background charged particles are concentrated. A coincidence with the electron spectrometer of 100 nsec is required, so most of the proton-proton events are already rejected by the electron trigger and will not be recorded. In this spectra the two detected particles cannot be separated in time by more than 20 ns. The peak at small TOF values corresponds to a proton associated with another particle (proton or deuteron) distributed in a 20 nsec window. At larger TOF values, the second peak corresponds to the two protons coming from the $(d, 2p)$ reaction. Its width originates from the 10% dispersion in the deuteron beam energy, the relative energy

TDC spectra for Ed = 200 MeV

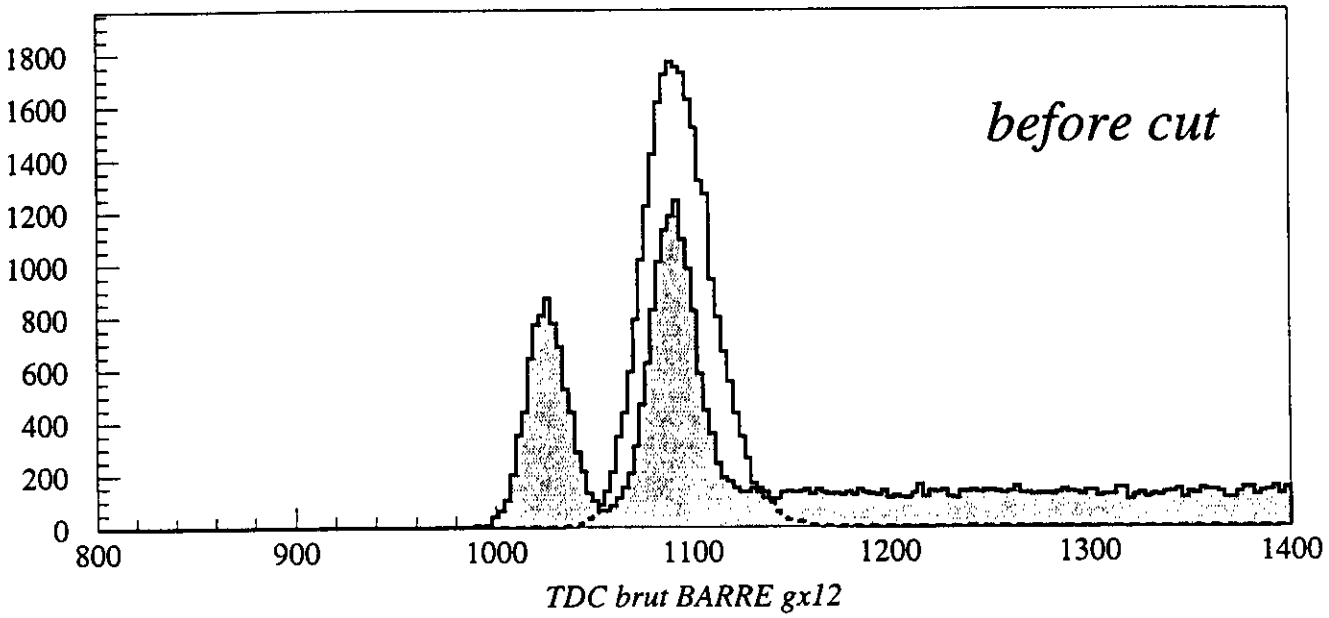

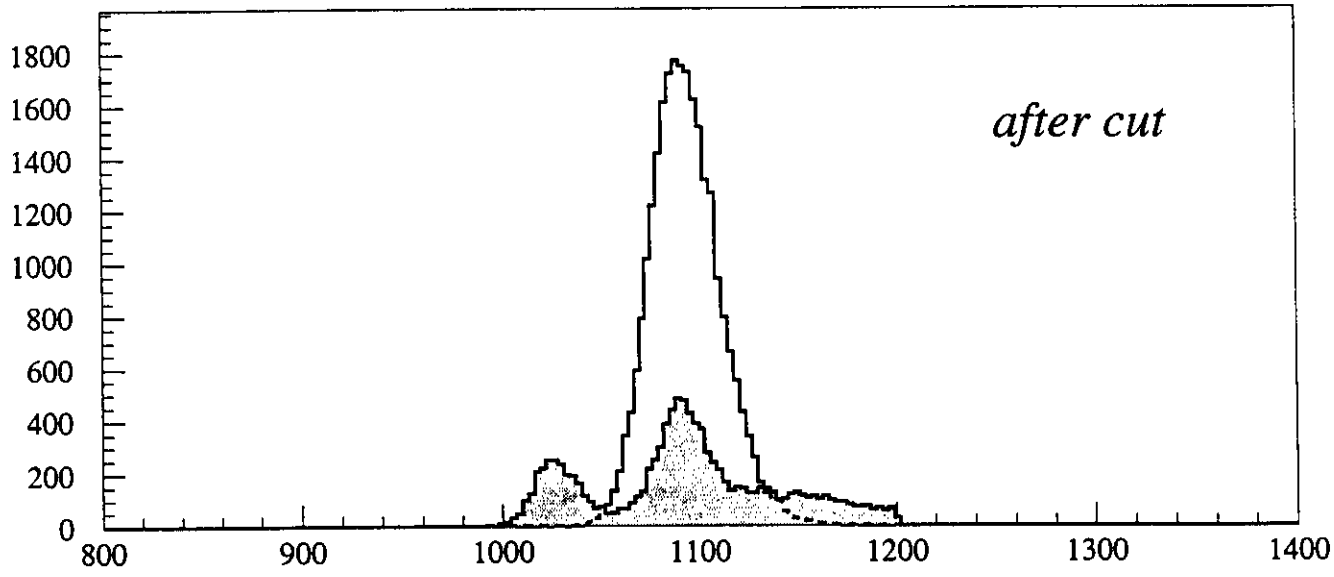

(0.05 nsec/chan.)

figure 12

of the pp pair, and from the resolution of the TOF measurement. The TOF cut is shown in figure 12b (a similar cut is applied on the first hodoscope). After these cuts (typically 5 ns wide) approximately 70% of the background events are rejected.

All dp background events are characterized by a multi-hit event (two particles) in the two front MWPCs. Each MWPC will be composed of three U-V planes with 1.2 mm wire spacing and rotated by 120°. A typical efficiency of 95% for one plane leads to an overall efficiency greater than 99% when two planes out of three are required. In the data treatment we assume that two particles with a relative distance smaller than 1 cm cannot be discriminated. This is a very conservative assumption but with the expected beam profile (larger than 2×10 cm^2 for protons), a reduction factor of 10 is obtained.

The veto detector placed behind the second hodoscope and after an absorber, stopping the protons originating from the $(d, 2p)$ of interest, detects background protons and deuterons. The events including such tagged particles can be rejected off-line. Considering the energy and angular spread of the beam, about 60% of these events are detected by the veto detector, resulting in another reduction factor of 3 for the background events.

In the last stage of the analysis, made when only CE events are supposedly remaining, the detection surface of the hodoscope is restricted to a circle in order to prevent geometrical asymmetries. The data are binned in the relevant kinematical variables such as q^2, E_x and ϕ. In particular, events with a small relative energy can be selected (a bin of 0-5 MeV has been chosen for the simulations). Finally, most (90%) of the remaining background events are located in the first bin of q, which is usually not used in the fitting procedure to extract the polarization coefficients.

In figure 13 is shown the percentage of dp background events to charge exchange events at all stages of the data analysis. As expected, the background event rate is lower at 400 MeV than at 200 MeV. Calculations have been made with the new design of the deuteron arm. With the electron arm in coincidence, the only significant contribution to the background is the deuteron-proton coincidence. The background contribution is reduced to less than 0.2 % of the charge exchange events in the worst case (200 MeV deuteron) after the full data analysis. This result is obtained with loose gates and is conservative. From this simulation, it appears that the off-line data analysis can easily reject backgrounds due to accidental coincidence events.

POLDER has to measure absolute charge exchange cross sections, which requires a precise determination of the incident deuteron flux. Random ep coincidences rep-

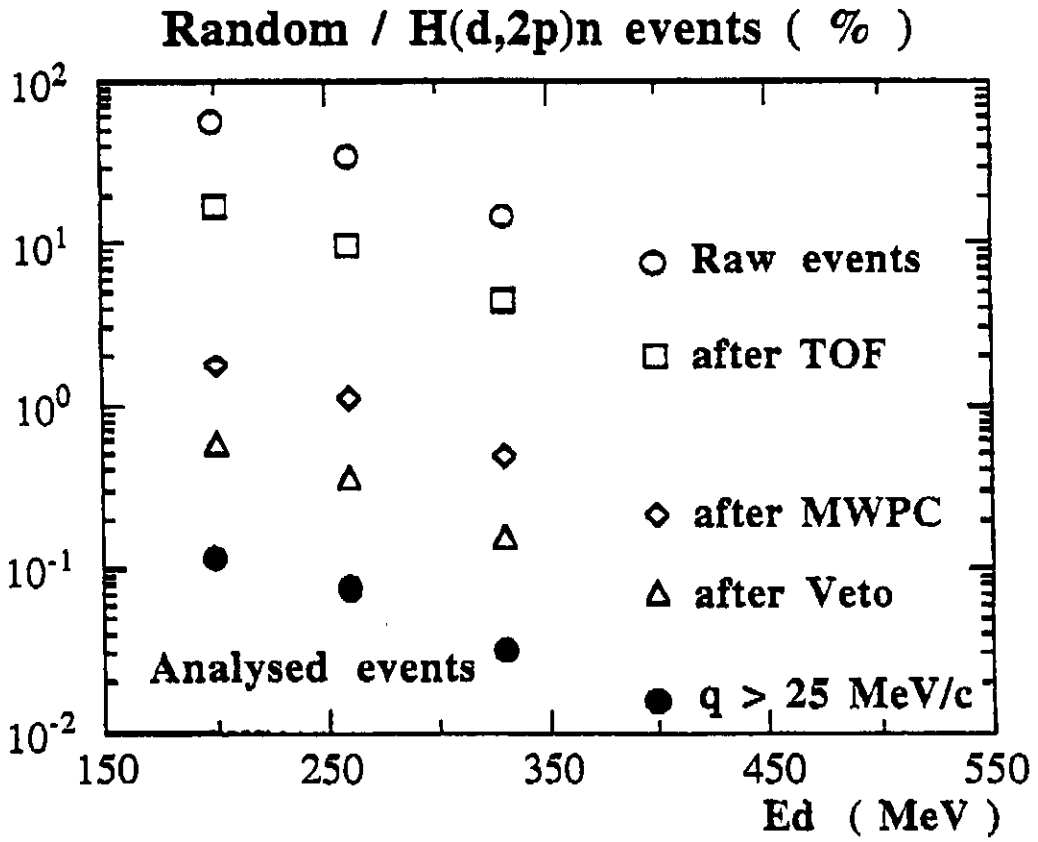
Random / H(d,2p)n events (%)
10^2
10^1
10^0
10^-1
10^-2
150
250
350
450
550
Ed (MeV)
Raw events
after TOF
after MWPC
after Veto
q > 25 MeV/c
Analysed events

figure 13

resent a contribution of about 3% of the number of incident deuterons at 200 MeV for a 100 nsec wide coincidence gate. To remove this background, TOF information between the electron and the proton/deuteron will be recorded (expected FWHM of 3−5 ns). Cuts in this time spectrum should allow a reduction by a factor larger than 10. Moreover, the energy deposited in the start scintillators will be useful in discriminating protons against deuterons after the magnetic channel. Finally the primary vertex (of the *e-d* scattering) can be reconstructed from the information in both spectrometers. Thus *e-p* coincidences should not contribute to the error in the determination of the absolute $(d, 2p)$ cross section at a level larger than 0.1 %.

7 Beam Time Estimate

In this section we will detail our beam time estimate and associated errors given in table 7.1.

7.1 Counting Rates

The cross section is calculated using relation (2.4) with a fixed angle of 60.5° for the deuteron spectrometer. The beam energy and electron angles for each value of momentum transfer, Q, are calculated from two-body kinematics. A solid angle of 6 msr for the HMS spectrometer was used, with the calculated mismatch factors to account for the incomplete overlap between the electron and deuteron channel acceptances.

The values of the structure functions $A(Q^2)$ are interpolated from the values of reference [1] and [47]. At the kinematics of this experiment, there is a discrepancy in the existing data, and we have chosen the smaller values of A to estimate the counting rates. It should be noted that in order to separate G_C and G_Q, the precision of the measured $A(Q^2)$ in this Q range should be improved. There exists an approved Hall A experiment to measure $A(Q^2)$ in the range $5.0 < Q < 12.4$ fm^{-1}. $B(Q^2)$ can be neglected at our kinematics.

A beam intensity of 100 μA and a useful target length of 10 cm will yield a luminosity of 3×10^{38} cm^{-2}s^{-1}. The radiative losses have been estimated to be about 25%. The coincident detection of the deuteron and electron should allow us to put a wide window on the electron energy spectrum, keeping the loss of events due to radiative processes to a minimum. The limiting factor is the momentum acceptance of the electron spectrometer.

7.2 Statistical Precision

The statistical precision of the t_{20} measurement is estimated from the polarimeter figures of merit (figure 12) measured in the calibration procedure. Systematic errors must be added (estimated to be of the order of 0.05 for t_{20}) as well as the error linked to the statistics recorded during the calibration runs (0.02 in our case).

Table 7.1

Statistical errors in the measurement of t_{20}. The calculation is performed with a beam intensity of 100 μA, a target length of 10 cm and a radiative correction factor of 0.75. The deuteron angle is fixed at 60.5°.

Q (fm^{-1})	T_d (MeV)	E_{Beam} (GeV)	$\theta_{elec.}$ (°)	$A(Q^2)$	Time (days)	N deuterons	F_{20}	Δt_{20}
4.0	170.	1.31	37	3×10^{-4}	1	$9.\times10^{6}$	0.011	0.03
4.4	200.	1.58	34	2×10^{-4}	2	$9.\times10^{6}$	0.013	0.03
5.0	260.	2.01	30.5	7×10^{-5}	4	5.7×10^{6}	0.011	0.04
5.6	330.	2.56	27	3×10^{-5}	8	$5.\times10^{6}$	0.009	0.05
6.2	400.	3.20	23.6	2×10^{-5}	9	$3.\times10^{6}$	0.008	0.08
6.8	480.	4.0	20.5	10^{-5}	10	1.4×10^{6}	0.006	0.14

Several factors have made the numbers in this table different from those in the previous proposal. The most significant gain comes from going to higher beam energies and therefore more forward electron angles. The deuteron channel acceptance has also been increased considerably, even though it could not fully overlap with the electron channel acceptance for our choice of beam energies. The number of required beam days is slightly smaller to that of our previous request, but with two additional points at 4.0 and 6.8 fm^{-1}. For this latter point the mismatch factor f is small (0.42), but we nevertheless propose this measurement since it is the maximum Q value reachable in this program. Since there is a significant overhead in setting up the apparatus we have proposed a program as complete as possible.

With this request, it will be possible to improve significantly the precision of the points measured at Bates near 4 fm^{-1}, and measure new points with good precision up to 6.8 fm^{-1} (see figure 1). In the original proposal, only one data point in the Bates range was proposed. In light of new preliminary data from Novosibirsk [12] which are in disagreement with the Bates data, we added one additional point at the lowest possible kinematics at which the polarimeter can operate with a good figure of merit.

7.3 Beam Time Request and Schedule

A small amount of additional beam time will also be required for tests, background reduction and counting rates checks. Also time is needed for beam energy changes. This leads to the following beam time request:

Preparation	144 hours
Physics	816 hours
Contingency	144 hours
	1104 hours (46 days)

We should be ready to install the experiment by the end of 1996. Ideally the schedule for the experiment would be five weeks for installation of the polarimeter and deuteron channel, one week for preparatory tests, and six weeks for the full set of measurements.

8 Comparison with Other Experiments

The recoiling deuteron polarization measurement, as proposed here, has so far [9] been the most efficient way to measure t_{20} and the proposed experiment will improve significantly on the overall figure of merit of the experiment performed recently at Bates.

An alternate technique to measure the same quantity is to scatter electrons off a polarized target. In this case one deals with a single arm scattering and only the analyzing power (T_{20}) has to be measured. Experiments based on an external cryogenic polarized target are very limited by the amount of beam this kind of target can withstand [7]. Even when used with large acceptance detectors, it is presently not competitive with the polarimeter technique. Another method has been pioneered at Novosibirsk [4, 5] using an internal target in a storage ring. Target technology is progressing steadily [6] and new measurements at moderate Q values are currently underway [12]. Using higher energy machines (in order to gain cross section) new viable experiments at high Q are under discussion[48].

We would like to stress that the combination of CEBAF and *POLDER* constitute, at the present time, the most competitive tool for t_{20} measurements. However even if other measurements become feasible in a similar Q range, it is important to get a data set as large as possible, considering the importance of the physics and the difficulty in controlling systematic errors in the different techniques.

Finally this experiment will also provide precise data for two other tensor polarization t_{22} and t_{21}. These data are less sensitive to the details of the models, but they provide other interesting combinations of the form factors.

9 Collaboration Responsibilities

The technical aspects which dictate the final choice of the Hall have been investigated. Support of the hall C staff for issues like the cryogenic target, electron spectrometer and data acquisition will be provided. The responsibilities from within the collaboration are distributed as follows:

Polarimeter: Grenoble-Saclay-Orsay-Saturne. Final tests and calibration of the polarimeter. This could involve changes in either the LH_2 or detection device. MIT/Bates might be involved in the safety aspects of the target.

Deuteron channel: Saclay–MIT/Bates–Hall C–IUCF–Grenoble. Final design of the optics and choice of the magnets. Magnets, power supplies and cooling water (Hall C and MIT/Bates). Construction of a new quadrupole and mechanics for the platform (Saclay–Grenoble)

LD_2 Target: CEBAF/Hall C–U Maryland–Basel. Upgrade of the existing Hall C target to a 400 W system. Design and construction of a dedicated scattering chamber.

Electron spectrometer: CEBAF/Hall C–Rutgers. Electron detection, connection with *POLDER*. Reconstruction of deuteron energy from electron arm information.

Data acquisition: CEBAF/Hall C–Rutgers–Grenoble–Saclay. Interconnection of the acquisition systems of *POLDER* and electron spectrometer.

Background estimates: U Maryland–Orsay–Rutgers. Simulations and estimates of shielding.

Figure Captions:

1: Predictions of various theoretical models for t_{20} as a function of the the momentum transfer to the deuteron, along with existing data.

2: Schematic lay-out of the t_{20} measurement at CEBAF (see text for details).

3: Trajectories in the deuteron transport channel calculated for deuterons produced at $\pm$ 4cm of the center of the primary LD_2 target.

4: Schematic view of proposed large rectangular aperture quad, used as Q2 in the deuteron channel.

5: Variation of $f(d\sigma/d\Omega_e)$ with beam energy, for fixed values of Q.

6: Artist's view of the *POLDER* polarimeter (see text for details).

7: Comparison of the experimental and simulated (see text) q and E_x spectra. Simulation inputs are the impulse approximation model, which has been shown to describe well the ^{1}H($\vec{d}$,2p)n reaction [39].

8: Total detection efficiency of the *POLDER* setup for the the ^{1}H($\vec{d}$,2p)n reaction in the excitation bin 0-5 MeV. The efficiency is shown for different runs of the calibration measurement at incident energies of 200-500 MeV and performed under very different experimental conditions. The mean value is drawn as solid straight lines as well as values at $\pm$ 1%.

9: Analyzing powers and unpolarized cross sections measured with the *POLDER* polarimeter at 200 and 400 MeV incident deuteron energies. The bin in excitation energy of the *pp* pair is 0-5 MeV.

10: Figures of merit extracted from POLDER calibration data, as a function of beam energy and integrated excitation energy E_x.

11: Single arm distributions of momentum, horizontal position and horizontal angle for high energy background protons from LD_2.

12: Simulation singles TOF spectrum expected in *POLDER*, based on calculated background rates. A hardware timing window of 100 ns between the electron and deuteron arms is assumed, as well as a 20 ns window between deuterons and the particles detected in the *POLDER* hodoscopes.

13: Percentage of background rates to good charge exchange events in *POLDER*, as calculated from the simulation, at each stage of data analysis.

References

[1] R.G. Arnold *et al.* , Phys. Rev. Lett. **35**, 776 (1975);
S. Platchtkov *et al.* , Nucl. Phys. **A510**, 740 (1990).

[2] S. Auffret *et al.* , Phys. Rev. Lett. **54**, 649 (1985);
P.E. Bosted *et al.* , Phys. Rev. C **42**, 38 (1990).

[3] M.E. Schulze *et al.* , Phys. Rev. Lett. **52**, 597 (1984).

[4] V.F. Dmitriev *et al.*, Phys. Lett. **157B**, 143 (1985).

[5] B.B. Voitsekhovskii *et al.* , JETP Lett. **43**, 733 (1986).

[6] R. Gilman *et al.* , Phys. Rev. Lett. **65**, 1733 (1990).

[7] B. Boden *et al.*, Z. Phys. C - Part. and Fields **49**, 175 (1991).

[8] M. Garçon, Nucl. Phys. **A508**, 445c. (1990).

[9] I. The *et al.* , Phys. Rev. Lett. **67**, 173 (1991);
M. Garçon *et al.* , Preprint DAPNIA/SPhN 93-19, to be published in Phys. Rev. C (April 1994).

[10] J.S. Réal, Thèse de l'Université Grenoble 1, ISN 94-04, 1994, unpublished;
S. Kox *et al.*, to be published in Nucl. Instr. and Methods A.(1994)

[11] J.M. Cameron *et al.*, Nucl. Inst. and Methods **A305**, 257 (1991).

[12] C.E. Jones, proceedings of the 14th European Conference on Few-Body Problems in Physics, Amsterdam, The Netherlands, 1993 (Argonne preprint # PHY-7659-ME-93).

[13] G.E. Brown and A.D. Jackson, *The Nucleon-Nucleon Interaction*, North-Holland Publishing, (Amsterdam, 1976).

[14] R. Machleidt, K. Holinde and Ch. Elster, Phys. Rep. **149**, 1 (1987).

[15] M.I. Haftel, L. Mathelitsch and H.F.K. Zingl, Phys. Rev. C **22**, 1285 (1980).

[16] V.M. Muzafarov and V.E. Troitskii, Sov. J. Nucl. Phys. **33**, 783 (1981).

[17] I.I. Belyantsev, V.K. Mitrjushkin, P.K. Rashidov, and S.V. Trubnikov, J. Phys. G: Nucl. Phys. **9**, 871 (1983).

[18] B. Mosconi and P. Ricci, Few-Body Syst. **6**, 63 (1989); *Erratum*, *ibid.* **8**, 159 (1990).

[19] R. Schiavilla and D.O. Riska, Phys. Rev. C **43**, 437 (1991).

[20] J. Pauschenwein, W. Plessas and L. Mathelitsch, Few-Body Systems, Suppl. **6**, 195 (1992).

[21] R. Schiavilla, V.R. Pandharipande and D.O. Riska, Phys. Rev. C **41**, 309 (1990).

[22] H. Henning, J. Adam, Jr. and P.U. Sauer, Few-Body Systems, Suppl. **5**, 133 (1992).

[23] A. Amroun *et al.*, Phys. Rev. Lett. **69**, 253 (1992).

[24] R.G. Arnold, C.E. Carlson, and F. Gross, Phys. Rev. C **21**, 1426 (1980).

[25] M.J. Zuilhof and J.A. Tjon, Phys. Rev. C **24**, 736 (1981); Phys. Rev. C **22**, 2369 (1980).

[26] E. Hummel and J.A. Tjon, Phys. Rev. C **42**, 423 (1990).

[27] E. Hummel and J.A. Tjon, Phys. Rev. C **49**, 21 (1994).

[28] N. K. Devine and S. Wallace, Phys. Rev. C **48**, R973 (1994).
See also N. Devine, Ph.D. thesis, University of Maryland, 1992, unpublished.

[29] M. Wakamatsu and W. Weise, Nucl. Phys. **A477**, 559 (1988).

[30] E.M. Nyman and D.O. Riska, Nucl. Phys. **A468**, 473 (1987).

[31] C.E. Carlson and F. Gross, Phys. Rev. Lett. **53**, 127 (1984).

[32] C.E. Carlson, Nucl. Phys. **A508**, 481c (1990).

[33] S.J. Brodsky and J.R. Hiller, Phys. Rev. D **46**, 2141 (1992).

[34] A. Kobushkin and A. Syamtomov, Phys. Rev. D **49**, 1637 (1994).

[35] G.G. Ohlsen, Rep. Prog. Phys. **35**, 717 (1972);
G.G. Ohlsen and P.W. Keaton, Jr, Nucl. Instr. Meth. **109**, 41 (1973).

[36] D.V. Bugg and C.Wilkin, Phys. Lett. **B152**, 37 (1985).

[37] T. Motobayashi *et al.*, Phys. Lett. **B233**, 69 (1989);
S. Kox *et al.*, Phys. Lett. **B266**, 264 (1991) ;
S. Kox *et al.*, Nucl. Phys. **A556**, 621 (1993).

[38] M. Garçon *et al.*, Nucl. Phys. **A458**, 287 (1986).

[39] J. Carbonell, M. Barbaro and C. Wilkin, Nucl. Phys. **A529** (1991) 653.

[40] E. Tomasi-Gustaffson *et al.*, LNS/Ph Report # **91-27** (1991), Saclay, unpublished.

[41] K.A.Aniol and V.Punjabi, Cebaf Tech. Note TN-91-024, Hall A Line of Sight Shielding.

[42] K.A.Aniol, Cebaf Tech. Note, Low Energy Neutron Shielding for Hall A detector hut.

[43] J.W. Lightbody and J.S. O'Connell, Comp. Phys. (May/June), 57 (1988).

[44] S. Freedman *et al.*, Phys. Rev. **C48**, 1864 (1993).

[45] J.E. Belz, Ph.D. thesis, California Institute of Technology, (1993).

[46] L.E. Wright and L. Tiator, Phys. Rev. **C26**, 2349 (1982).

[47] J. Elias *et al.*, Phys. Rev. **117**, 2075 (1969).

[48] HERMES proposal.

Proposal: PR-93-003, Hall A/C

Spokespersons: S. Kox, E.J. Beise

Title: Measurement of the Deuteron Tensor Polarization at Large Momentum Transfer in D $(e, e'\vec{d})$

Motivation:

The primary goal of the proposed experiment is to separate the charge and quadrupole form factors of the deuteron in the momentum transfer range of 4.4 to 6.2 fm^{-1}. This momentum transfer range is particularly interesting since the charge form factor goes through zero in this region; and consequently it is very sensitive to the deuteron wave function, isoscalar meson exchange current and relativistic effects.

Measurement and Feasibility:

The measurement makes use of electron scattering from a high- power (500W) liquid deuterium target and a novel polarimeter technique. The Hall C cryotarget must be upgraded from a 250-watt capability to accommodate this experiment. No target upgrade is necessary if the experiment is scheduled for Hall A. The polarimeter must be calibrated with tensor polarized deuterons at Saturne II. From measurements of efficiency and analyzing power, it appears that this new polarimeter has the highest figure of merit of any deuteron tensor polarimeter in the few hundred MeV energy range. However, the in-line geometry, lack of redundant particle identification, and the requirement of an absolute efficiency measurement in a high-background environment make this a very difficult experiment. Complete simulations need to be performed so that the feasibility of the method can be fully assessed.

Issues:

There is clear physics interest in this proposed measurement. There needs to be an optimization of the target, deuteron channel and choice of beam energy, plus full simulations of the backgrounds.

A QQD channel will be used to focus deuterons onto the polarimeter. This channel must be matched to either the HRS (Hall A) or the HMS (Hall C). The PAC was not convinced that the deuteron channel was optimized for this measurement. For example, the highest electron energy proposed was 2 GeV rather than 4 GeV. If a deuteron channel could be matched to the electron spectrometer for a 4 GeV incident beam, a factor of 4 improvement in figure of merit could be realized. The proponents should consider a possible optimization scheme for a 4 GeV beam. Complete background simulations are necessary. Experience with deuteron tensor polarimeters indicates that the figure of merit can be seriously compromised by unexpected background rates in various detectors. The collaboration should provide a complete simulation of possible backgrounds to ensure that the figure of merit of the experiment is achievable.

Manpower:

The collaboration consists of an international collaboration with extensive experience in polarization measurements and electron scattering experiments.

Recommendation:

Defer

HAZARD IDENTIFICATION CHECKLIST

CEBAF Experiment: Measurement of Deuteron Tensor Pol. at Large Q^2 in D(ee'$\vec{d}$) scattering Date: April 14, 1994

Check all items for which there is an anticipated need—do not check items that are part of the CEBAF standard experiment (HRSE, HRSH, CLAS, HMS, SOS in standard configurations).

Cryogenics
- ____ beamline magnets
- ____ analysis magnets
- ✓ target
- ____ drift chambers
- ____ other

Electrical Equipment
- ____ cryo/electrical devices
- ____ capacitor banks
- ____ high voltage
- ____ exposed equipment

Radioactive/Hazardous Materials
List any radioactive or hazadorous/ toxic materials planned for use:

Pressure Vessels
- ____ inside diameter
- ____ operating pressure
- ____ window material
- ____ window thickness

Flammable Gas or Liquids
(incl. target)
type: lD_2
flow rate:
capacity: 400 W
also lH_2 tgt in polarimeter (feasibility)

Other Target Materials
- ___ Beryllium (Be)
- ___ Lithium (Li)
- ___ Mercury (Hg)
- ___ Lead (Pb)
- ___ Tungsten (W)
- ___ Uranium (U)
- ___ Other (list below)

Vacuum Vessels
- ~60cm inside diameter
- ____ operating pressure
- ____ window material
- ____ window thickness

Radioactive Sources
- ____ permanent installation
- ____ temporary use

type:
strength:

Large Mech. Structure/System
- ____ lifting devices
- ____ motion controllers
- ✓ scaffolding or elevated platforms
- ____ other

Lasers
type:
wattage:
class:

Installation
- ____ permanent
- ____ temporary

Use
- ____ calibration
- ____ alignment

Hazardous Materials
- ___ cyanide plating materials
- ___ scintillation oil (from)
- ___ PCBs
- ___ methane
- ___ TMAE
- ___ TEA
- ___ photographic developers
- ___ other (list below)

Notes:
Exp requires installation of new magnetic channel, shielding and polarimeter